

# Emergent criticality in fully frustrated quantum magnets

Yuchen Fan,<sup>1</sup> Ning Xi,<sup>2</sup> Changle Liu,<sup>3,4</sup> Bruce Normand,<sup>5,6</sup> and Rong Yu<sup>2,7</sup>

<sup>1</sup>*Beijing National Laboratory for Condensed Matter Physics and Institute of Physics, Chinese Academy of Sciences, Beijing, 100190, China*

<sup>2</sup>*Department of Physics and Beijing Key Laboratory of Opto-electronic Functional Materials and Micro-nano Devices, Renmin University of China, Beijing 100872, China*

<sup>3</sup>*School of Engineering, Dali University, Dali, Yunnan 671003, China*

<sup>4</sup>*Shenzhen Institute for Quantum Science and Technology and Department of Physics, Southern University of Science and Technology, Shenzhen 518055, China*

<sup>5</sup>*Laboratory for Theoretical and Computational Physics, Paul Scherrer Institute, CH-5232 Villigen-PSI, Switzerland*

<sup>6</sup>*Institute of Physics, Ecole Polytechnique Fédérale de Lausanne (EPFL), CH-1015 Lausanne, Switzerland*

<sup>7</sup>*Key Laboratory of Quantum State Construction and Manipulation (Ministry of Education), Renmin University of China, Beijing 100872, China*

Phase transitions in condensed matter are often linked to exotic emergent properties. We study the fully frustrated bilayer Heisenberg antiferromagnet to demonstrate that an applied magnetic field creates a novel emergent criticality. The quantum phase diagram contains four states, the DS (singlets on every interlayer dimer bond), DTAF (all triplets with antiferromagnetic order), TC (a singlet-triplet checkerboard) and FM (saturated ferromagnet). The thermal phase diagram is dominated by a wall of discontinuities extending from the zero-field DTAF-DS transition to a quantum critical endpoint where the field drives the DTAF and TC into the FM. This first-order wall is terminated at finite temperatures by a line of critical points, where the Berezinskii-Kosterlitz-Thouless (BKT) transition of the DTAF and the thermal Ising transition of the TC also terminate. We demonstrate by quantum Monte Carlo simulations that the BKT transition does not change the Ising nature of the DTAF-DS critical line. By contrast, the combination of symmetries merging on the multicritical DTAF-TC line leads to a 4-state Potts universality not contained in the microscopic Hamiltonian, which we associate with the Ashkin-Teller model. Our results represent a systematic step in understanding emergent phenomena in quantum magnetic materials including the “Shastry-Sutherland compound”  $\text{SrCu}_2(\text{BO}_3)_2$ .

Classical and quantum field theories, formulated to capture the low-energy, long-wavelength behaviour of a system, have a foundational role in theoretical physics. At a continuous classical or quantum phase transition (QPT), the characteristic energy scale vanishes and the correlation length diverges, ensuring a profound connection between field theories and the statistical mechanics of critical phenomena.<sup>1</sup> In both situations, the microscopic details become irrelevant and the critical properties of the system are dictated only by global and scale-invariant characteristics such as the dimensionality, symmetry and sometimes the topology. Because these most

basic attributes are all discrete, field theories are readily classified and phase transitions can be categorized by their universality class.

One of the organizing principles of modern condensed matter is the concept of “emergence,” meaning large-scale patterns of behaviour that cannot be predicted from a knowledge of the short-range interactions. Quantum magnetic materials and models are widely recognized for the wealth of emergent phenomena they exhibit at low energies, which include multiple types of fractional excitation and of quantum spin liquid.<sup>2</sup> Many more phenomena emerge when a system is driven into the critical regime around a phase transition.<sup>3</sup> Beyond the continuous (second-order) transitions that are now well studied in experiment,<sup>4,5</sup> theory predicts that the order parameters of two phases with unrelated symmetries can vanish continuously and simultaneously. This deconfined quantum critical point (DQCP),<sup>6,7</sup> or multicritical point,<sup>8,9</sup> should be accompanied by emergent fractional excitations, exhibit unconventional critical scaling<sup>10</sup> and possess an enhanced continuous symmetry. More generally, emergent enhanced symmetries have recently been discussed at a first-order transition<sup>11</sup> and at topological phase transitions.<sup>12,13</sup>

The many-body states of quantum spin systems can be altered by a variety of experimental methods, including an applied magnetic field,<sup>4</sup> a hydrostatic pressure<sup>5,14</sup> and controlled substitutional disorder,<sup>15</sup> to obtain a wide range of possibilities for the investigation of phase transitions and related emergent phenomena. The field-induced magnetic order observed in dimerized spin systems can be described as a Bose-Einstein condensation of triplet excitations into the singlet ground state,<sup>4</sup> while the pressure-induced transition<sup>5</sup> is a triplet condensation in the 3D XY universality class. It was pointed out recently that critical phenomena in quantum magnets are not restricted to second-order QPTs, but that the combination of quantum and thermal fluctuations can produce a critical point when the QPT is first-order.<sup>16</sup> Using the  $S = 1/2$  “fully frustrated bilayer” (FFB) model shown in Fig. 1a, it was found that the discontinuity across the QPT, between the dimer-singlet

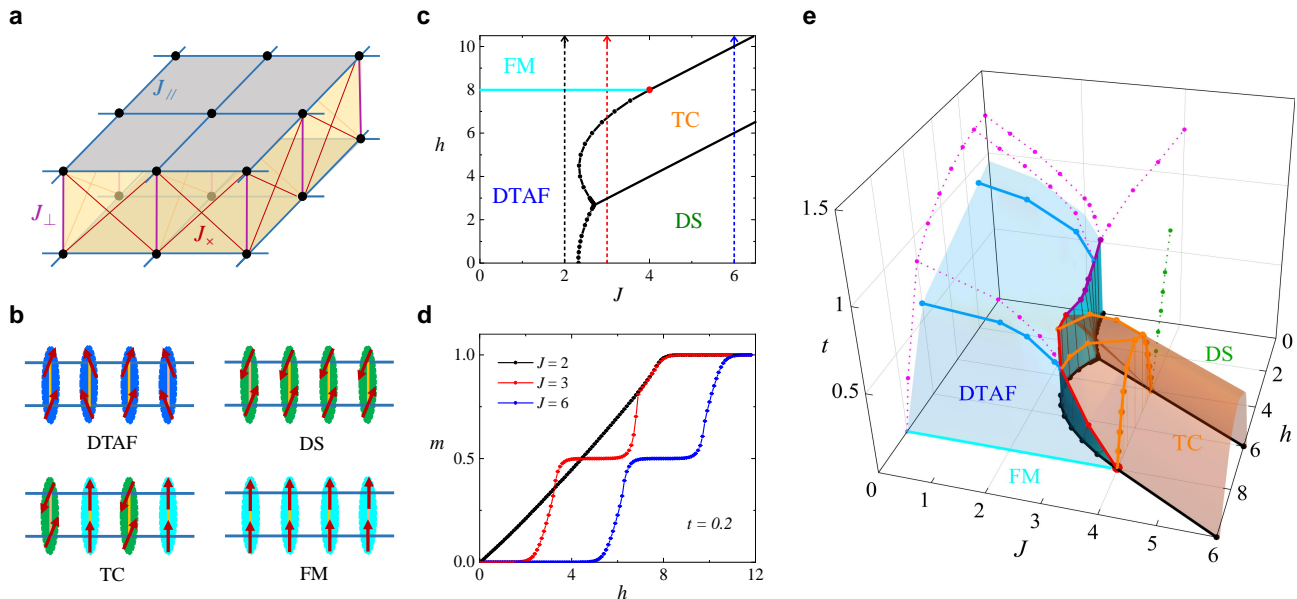


**FIG. 1. Phase diagram of the fully frustrated bilayer Heisenberg model in an applied magnetic field.** **a** FFB model. Quantum spins ( $S = 1/2$ ) are located at every site of a pair of square lattices. The interlayer dimer unit has magnetic interaction  $J_{\perp}$ , the intralayer interaction is  $J_{\parallel}$  and the interlayer interaction between adjacent sites is  $J_x$ ; all three interactions are antiferromagnetic (AF) and of Heisenberg type. **b** Representations of the four different ground states in an applied field, the dimer triplet antiferromagnet (DTAF), dimer singlet (DS), checkerboard triplon crystal (TC) and fully polarized ferromagnet (FM). **c** Ground-state phase diagram obtained by the iPESS method. Apart from the field-driven DTAF-FM transition (cyan line), which is continuous, all other transitions are first-order (black lines). The red circle marks the quantum critical endpoint (QCEP) at  $J = 4$  and  $h = 8$ . **d** Magnetization shown as a function of  $J$  at low temperature ( $t = 0.2$ ), calculated by quantum Monte Carlo (QMC) for a system of size  $L \times L$  dimers, with  $L = 24$ . The half-magnetization plateau characterizes the TC state. **e** Thermal phase diagram. Long-ranged DTAF and FM order is present only at zero temperature. The TC order parameter persists at finite temperatures, and this order melts continuously at the orange surface. The wall of discontinuities in the triplet density that separates the DTAF and DS phases terminates at a line of Ising critical points (purple) at finite temperatures, while the wall separating the DTAF and TC phases terminates at a line of emergent multicritical points (red). Each point on the red line is simultaneously the endpoint of a BKT transition of the DTAF (blue line with stars) and of a thermal Ising transition of the TC (orange), and exhibits an emergent 4-state Potts criticality. At high fields, the line of emergent multicritical points terminates at the QCEP (red circle). The magenta and green dashed lines mark characteristic crossover temperatures determined by computing the specific heat.

and dimer-triplet phases (DS and DTAF in Fig. 1b), decreases with increasing temperature and terminates at a finite-temperature critical point. In this minimal model, there is no spontaneous symmetry-breaking across the line of discontinuities (meaning at  $T > 0$ , by the Mermin-Wagner theorem) and the extent of singlet-triplet order provides a quantum magnetic analogue of the liquid-gas transition, the two-component nature conferring an Ising universality.<sup>17</sup>

This type of physics and its extensions have recently been pursued in a number of frustrated quantum spin models,<sup>18–20</sup> but came to the fore when it was shown to be the origin of critical-point behaviour found<sup>21</sup> in specific-heat measurements on the frustrated quantum antiferromagnet  $\text{SrCu}_2(\text{BO}_3)_2$ . This compound provides a remarkably faithful realization of the Shastry-Sutherland model (SSM),<sup>22</sup> not only at ambient pressure<sup>23</sup> but also in its pressure-induced QPTs.<sup>14</sup> However, the first-order QPT in  $\text{SrCu}_2(\text{BO}_3)_2$  and the SSM separates a DS phase from a plaquette-singlet phase, which does have long-

ranged order at low temperatures and a continuous thermal transition,<sup>21</sup> making the situation more complex than the FFB.  $\text{SrCu}_2(\text{BO}_3)_2$  also shows a complex cascade of QPTs in an applied magnetic field,<sup>23,24</sup> raising important questions about the nature of criticality under combined fields and pressures. The possibilities range from emergent enhanced symmetries and emergent types of multicriticality to the appearance of a DQCP suggested by theory<sup>25</sup> and experiment.<sup>26</sup>

Here we look more deeply into the FFB model to study how its phases and phase transitions evolve in an applied magnetic field. The field enriches the phase diagram, turning the dimer-triplet state into a Berezinskii-Kosterlitz-Thouless (BKT) phase with quasi-long-ranged order (qLRO), and the DS state into a checkerboard triplon crystal (TC) phase with LRO at finite temperatures. The Ising critical point becomes a critical line, first retaining its Ising character but then gaining an emergent 4-state Potts symmetry on the multicritical phase boundary to the TC regime, before terminating at a quantum

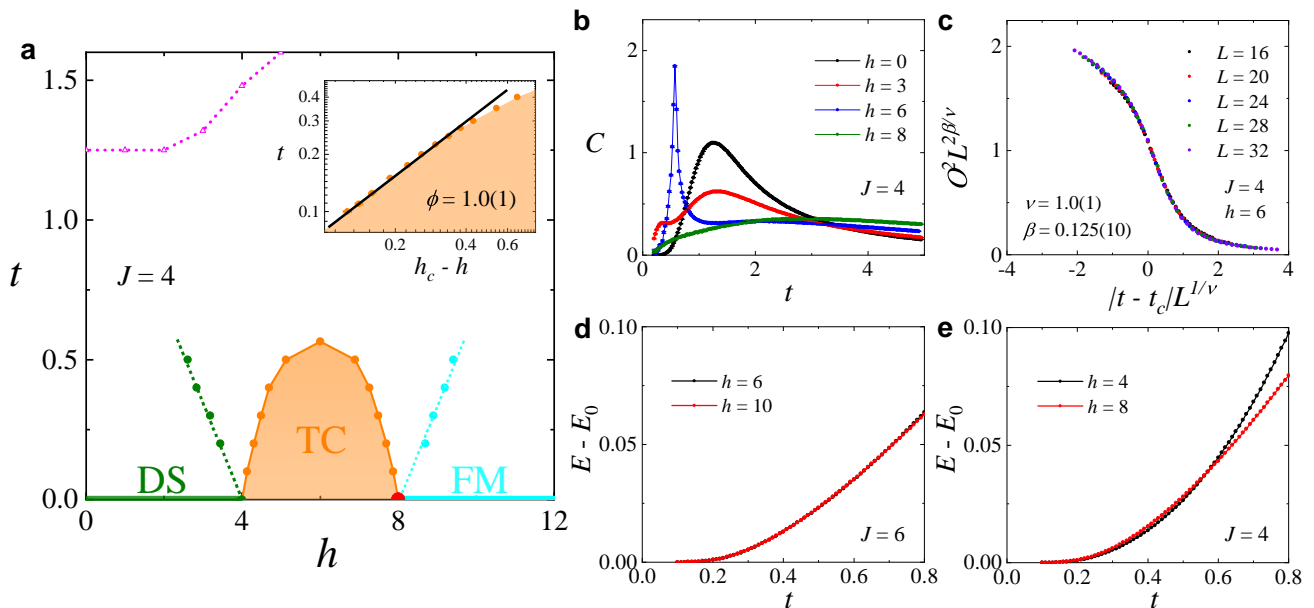


FIG. 2. **Physics of the DS and TC phases, and at the QCEP.** **a**  $(h, t)$  phase diagram of the FFB model at  $J = 4.0$ . The dashed green line shows the gap of the DS phase, the dashed cyan line the FM gap, the dashed magenta line the characteristic crossover temperature determined from the specific heat and the solid orange line the TC ordering temperature. The inset shows that the field-scaling exponent is  $\phi = 1$ ; the model does not have 2+1D Ising universality because the  $t = 0$  transition is first-order. **b** Specific heat,  $C(t)$ , shown for a number of applied field values. The peak temperatures are used to determine the phase-boundary (orange) and crossover (magenta) lines in panel a. **c** Ising nature of the thermal transition of the TC phase, shown by scaling collapse of the order parameter,  $O(t, L)$ , calculated at  $J = 4$  and  $h = 6$  for systems of linear size  $L$ . The critical exponents are fully compatible with the Ising values  $\nu = 1$  and  $\beta = 1/8$ . **d** Thermal energy,  $E(t) - E_0$ , computed with  $L = 24$  and shown at the points  $(J, h) = (6, 6)$  and  $(J, h) = (6, 10)$ , which lie respectively on the zero-temperature first-order DS-TC and TC-FM lines. The exponential form arises due to the gapped nature of both phases and appears identical as a consequence of particle-hole symmetry about triplet density  $n_t = 1/2$ . **e**  $E(t) - E_0$  at the points  $(J, h) = (4, 4)$ , on the DS-TC zero-temperature first-order line, and  $(J, h) = (4, 8)$ , which is the QCEP. The change in exponential form indicates a violation of particle-hole symmetry due to the presence of low-energy spin-wave excitations at the QCEP.

critical endpoint (QCEP). All our thermal calculations are performed using large-scale quantum Monte Carlo (QMC) methods enabled by the recent qualitative breakthrough that the fully frustrated system formulated in the dimer basis has no sign problem. We map the quantum FFB model to a classical equivalent and then to the Ashkin-Teller model in order to trace the origin of emergent criticality, and hence to shed light on its possible appearance in highly frustrated quantum magnetic materials such as  $\text{SrCu}_2(\text{BO}_3)_2$ .

## Results

The Hamiltonian of the FFB model is

$$\mathcal{H} = \sum_i J_{\perp} \vec{S}_{i,1} \cdot \vec{S}_{i,2} - H \sum_{i,m=1,2} S_{i,m}^z \quad (1)$$

$$+ \sum_{\langle i,j \rangle, m=1,2} \left[ J_{\parallel} \vec{S}_{i,m} \cdot \vec{S}_{j,m} + J_{\times} \vec{S}_{i,m} \cdot \vec{S}_{j,\bar{m}} \right],$$

where  $\vec{S}_{i,m}$  is a quantum  $S = 1/2$  spin at site  $i$  and layer  $m$  of the square-lattice bilayer shown in Fig. 1a,  $H$  is the applied magnetic field and the antiferromagnetic (AF) Heisenberg interactions are  $J_{\perp}$  on the inter-layer dimer bond,  $J_{\parallel}$  within each square lattice and  $J_{\times}$

between next-neighbour interlayer sites, which frustrates  $J_{\parallel}$ . We consider only the fully frustrated case,  $J_{\times} = J_{\parallel}$ , where the model can be rewritten in the dimer basis as

$$\mathcal{H} = J_{\parallel} \sum_{i,j} \vec{T}_i \cdot \vec{T}_j + J_{\perp} \sum_i \left( \frac{1}{2} \vec{T}_i^2 - \frac{3}{4} \right) - H \sum_i T_i^z, \quad (2)$$

with  $\vec{T}_i = \vec{S}_{i,1} + \vec{S}_{i,2}$  the total spin of each dimer;  $\vec{T}_i^2$  is proportional to the spin-triplet density and is locally conserved, meaning on every dimer,  $i$ . This is the property that causes the sign problem, which conventionally accompanies QMC simulations on frustrated spin systems, to be completely absent.<sup>27,28</sup> Thus we can use the stochastic series expansion (SSE) algorithm<sup>29</sup> to obtain highly accurate simulation results for square-lattice dimensions  $L \times L$  up to a linear size of  $L = 40$ . We take  $J_{\parallel}$  as the unit of energy and define the reduced coupling  $J = J_{\perp}/J_{\parallel}$ , reduced field  $h = H/J_{\parallel}$  and reduced temperature  $t = T/J_{\parallel}$ , with the lowest temperature we access being  $t = 0.1$ . To complement these thermal results, we calculate the quantum ( $t = 0$ ) phase diagram of the FFB in a field by applying the tensor-network method of infinite Projected Entangled Simplex States (iPESS),<sup>30</sup> as summarized in the Methods section. The FFB model

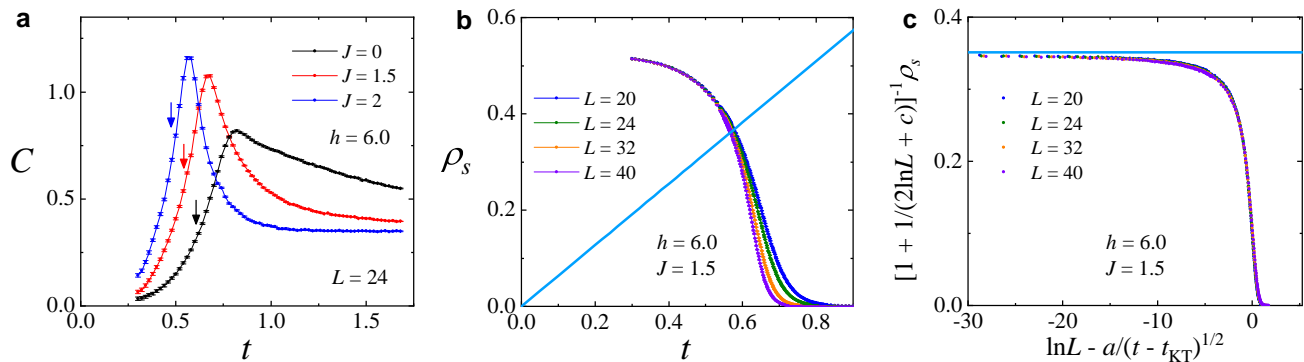


FIG. 3. **Physics of the DTAF phase.** **a** Thermodynamic properties of the DTAF, illustrated by the specific heat,  $C(T)$ , at  $h = 6$  for three different  $J$  values. The centre of the single broad peak gives a characteristic crossover temperature that lies above the BKT transition (coloured arrows). **b** Spin stiffness,  $\rho_s(t)$ , computed for systems of different sizes,  $L$ , at  $h = 6$  and  $J = 1.5$ . The BKT transition temperature,  $t_{\text{KT}}$ , is determined from the crossing point of  $\rho_s(t)$  with the linear function  $2t/\pi$  (cyan line) in the limit  $L \rightarrow \infty$ . **c** Finite-size scaling of the spin stiffness near the BKT transition, illustrated by its collapse according to the form  $\rho_s(t, L) = [1 + 1/(2 \ln L + c)] F_\rho(\ln L - a/\sqrt{t - t_{\text{KT}}})$ , where  $F_\rho$  is a scaling function. We extract the parameters  $a = 1.1 \pm 0.05$ ,  $c = 0.05 \pm 0.02$  and  $t_{\text{KT}} = 0.549 \pm 0.002$ .

has been studied in detail by SSE QMC at zero field,<sup>16</sup> and here we reveal the complex and emergent phenomena induced by the magnetic field. Some properties of the FFB in a field have been investigated by Richter and coworkers,<sup>31–33</sup> although these authors did not discuss the full phase diagram or emergent critical properties.

We begin by using iPESS to identify the four ground states of the model illustrated schematically in Fig. 1b. A straightforward energy comparison, described in Sec. S1 of the Supplementary Information (SI),<sup>34</sup> yields the  $t = 0$  phase diagram shown in Fig. 1c. The DS and dimer-triplet antiferromagnet (DTAF) states are familiar at zero field. Beyond a finite field, the DS is driven into the intermediate TC state, of alternating dimer singlets and field-aligned triplets, and the magnetization shows a plateau at half of its saturation value (Fig. 1d).<sup>32</sup> Sufficiently strong fields cause a full polarization of the DTAF and TC phases into the FM state. Because only the DTAF and FM phases have the same triplet density ( $n_t = 1$ ), every phase boundary in Fig. 1c is first-order, other than the line of continuous DTAF-FM transitions. This line terminates at a QCEP at  $J = 4$  and  $h = 8$ , where it meets the first-order phase boundary of the TC state.

Figure 1e shows the thermal phase diagram we obtain from our SSE QMC simulations. Only the TC phase has a LRO, which is terminated at a thermal transition (orange surface), although the DTAF has qLRO that is lost at a BKT transition (blue). The first-order DS-TC and TC-FM transitions become continuous at any finite temperature, an unconventional property we give the simple terminology “zero-temperature first-order line.” The first-order DTAF-DS and DTAF-TC lines persist to finite temperatures, forming a wall of discontinuities across the phase diagram, which is terminated by a (multi)critical line whose nature is the primary focus of our work.

To analyse the rich variety of phenomena on display

in Fig. 1e, we start on the DS side by considering the field-induced behaviour at fixed  $J = 4$  (Fig. 2a). The DS phase has no order parameter, but can be characterized by the dimer spin correlation.<sup>21</sup> At finite fields, the average of the three Zeeman-split triplon branches determines the position of the broad maximum in the specific heat (Fig. 2b), while the closure of the gap to the lowest triplon sets the DS-TC transition, shown in Fig. 1c. At  $J = 4$  and  $t = 0$ , the ground state undergoes first-order transitions from DS to TC at  $h = 4$  and TC to FM at  $h = 8$ , where the TC phase supports true LRO and thus has a continuous thermal phase transition at any point on the orange surface in Fig. 1e. By the scaling-collapse analysis presented in Fig. 2c and described in the Methods section, we show that this transition has the critical exponents of Ising universality,  $\nu = 1$  and  $\beta = 1/8$ , as might be anticipated from the twofold degeneracy (i.e. broken  $Z_2$  sublattice symmetry) of the checkerboard TC state.

We reiterate the curious nature of the critical surface of the TC phase at the DS and FM transitions, which changes from second- to first-order precisely at  $t = 0$ . The termination of a second-order line on a first-order one is known as a critical endpoint,<sup>35</sup> and a second-order line turning first-order is a tricritical point, but the DS-TC and TC-FM boundaries lack a first-order surface (*cf.* the QCEP at  $(J = 4, h = 8)$ ) or half-surface; thus we use instead the term zero-temperature first-order line. The physics of the DS-TC line is that any state excluding nearest-neighbour triplon pairs minimizes the energy, resulting in a highly degenerate ground state.<sup>31–33</sup> Away from the line, these states form low-energy excitations, while excitations containing at least one triplon pair have a gap of order  $J_{\parallel}$ , and these two types of process account for the two peaks in  $C(t)$  (Fig. 2b). Exactly analogous behaviour is observed around the TC-FM line as a consequence of particle-hole symmetry about  $n_t = 1/2$ . By

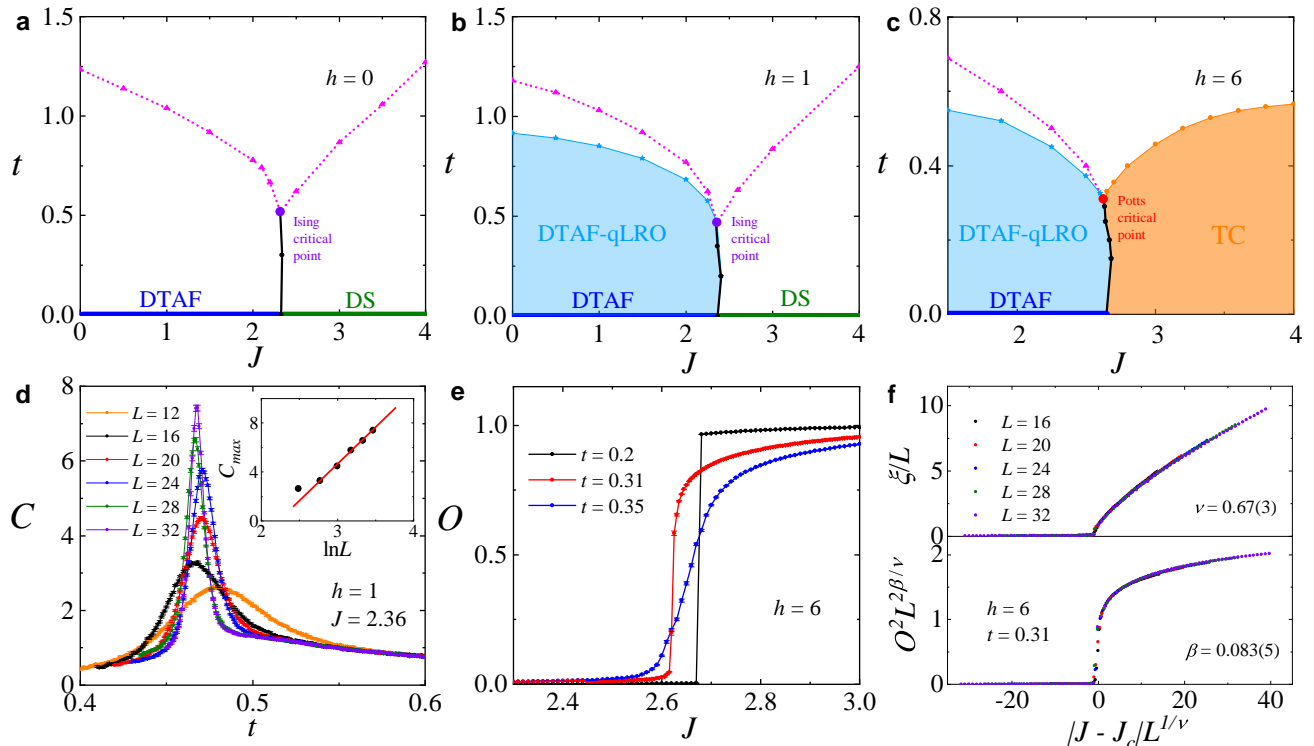


FIG. 4. **Physics of the (multi)critical point.** **a-c** Phase diagrams of the FFB model in the  $(J, t)$  plane at  $h = 0$  (a),  $h = 1$  (b) and  $h = 6$  (c). Black lines in each panel mark the first-order transition determined by the discontinuity in the triplet density. Magenta curves show crossover temperatures determined from the specific-heat peaks at each value of  $h$  and  $J$ . Blue lines and stars mark the BKT transition of the DTAF, below which the system exhibits qLRO. Orange lines and circles show the continuous thermal transition of the TC. At each field, all of the transition and crossover lines meet at a critical point that terminates the line of first-order transitions: this point is located at  $(J_c, t_c) = (2.315(1), 0.517(3))$  for  $h = 0$ ,<sup>16</sup>  $(2.36(1), 0.47(1))$  for  $h = 1$  and  $(2.624(4), 0.308(5))$  for  $h = 6$ , and has either Ising (purple circle) or 4-state Potts universality (red circle). **d** Specific heat,  $C(t)$ , calculated at  $J = J_c$  for  $h = 1$  using a range of system sizes,  $L$ . The sharpening of the peak with increasing  $L$  signals a continuous transition and the scaling of the peak value,  $C_{\max}$ , with  $\ln L$  (inset) indicates that the transition in the low-field regime is in the same 2D Ising universality class as the  $h = 0$  case. **e** Order parameter,  $O$ , of the TC phase calculated with  $L = 24$  for  $h = 6$  and shown as a function of  $J$  near the emergent (multi)critical point for three temperatures below, at and above  $t_c$ . **f** Scaling collapse of the finite-size correlation length,  $\xi$ , and the order parameter,  $O$ , across the emergent (multi)critical point. The critical exponents estimated from these two types of data collapse are  $\nu = 0.67 \pm 0.03$  and  $\beta = 0.083 \pm 0.005$ , which are fully consistent with 4-state Potts universality.

contrast, the TC-DTAF transition remains first-order up to a finite temperature, where the TC surface meets the line of critical points to establish the emergent criticality we analyse below.

Finally, to investigate the QCEP, defined as the termination point of a line of continuous QPTs (the DTAF-FM line), we characterize the low-energy excitation spectrum by computing the thermal energy,  $E(t) - E_0$ , at different points on the zero-temperature first-order lines. As Fig. 2d shows for the two transitions at  $J = 6$ ,  $E(t)$  has the same exponential form, indicating gapped excitations above the ground manifold, with the same prefactor, thereby respecting the particle-hole symmetry. However, in Fig. 2e we observe a departure from this symmetry when the QCEP is compared with its counterpart ( $h = 4$ ), with additional thermal energy at  $t \lesssim 0.5$  suggesting low-energy AF spin-wave fluctuations, in finite-

sized regimes of the neighbouring DTAF phase, appearing within the gap.

Turning to the DTAF side of the phase diagram (Fig. 1e), the field breaks the  $SU(2)$  spin symmetry down to  $U(1)$  and the DTAF phase supports qLRO below a finite-temperature BKT transition.<sup>36,37</sup> In Fig. 3a we use the specific heat to show that the thermodynamic properties of the DTAF phase, computed at  $h = 6$  for a number of  $J$  values, remain similar to those at  $h = 0$ , with a single peak marking a characteristic crossover temperature. An accurate determination of  $t_{KT}$  can be obtained<sup>38,39</sup> from the finite-size scaling of the spin stiffness,  $\rho_s(t)$ , as we explain in the Methods section and show in Figs. 3b and 3c. As expected,<sup>17</sup>  $t_{KT}$  is not reflected in the conventional thermodynamic response (Fig. 3a), lying systematically beneath the crossover such that the two temperatures form two sets of surfaces that meet along the

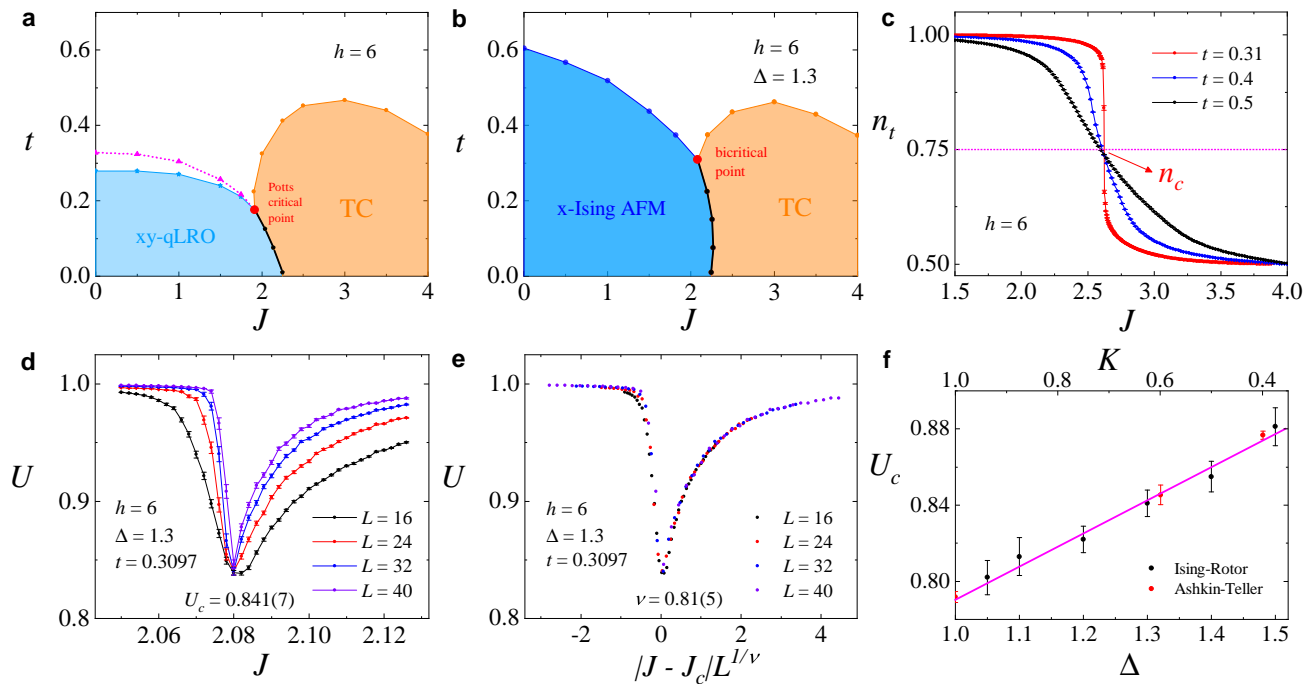


FIG. 5. **Classical model, spin-anisotropic model and Ashkin-Teller model.** **a** Phase diagram of the classical spin-rotor model extracted from the FFB model, shown at  $h = 6$ . **b** Phase diagram of the classical model with spin anisotropy, shown at  $h = 6$  with  $\Delta = 1.3$  (weak Ising anisotropy). The qLRO of the DTAF phase becomes a true LRO with a thermal Ising transition occurring at a rather higher ordering temperature. Because the TC phase retains its Ising transition, the emergent critical point becomes a bicritical point (red circle) where the two Ising transition lines meet at  $(J_c, t_c) = (2.0792(14), 0.3097(8))$ . **c** Triplet density,  $n_t$ , computed for  $L = 24$  and shown as a function of  $J$  for various temperatures at  $h = 6$ .  $n_t = 0.75$  at the multicritical point and reflects the approximate particle-hole symmetry between the DTAF and TC phases at their transition. **d** Binder cumulant,  $U$ , computed as a function of  $J$  across the bicritical point with  $h = 6$  and  $\Delta = 1.3$  for a range of system sizes.  $J_c = 2.0792 \pm 0.0014$  is determined from the touching point of the Binder-cumulant curves. **e** Collapse of the Binder-cumulant data shown in panel d, from which we estimate the non-universal critical exponent  $\nu = 0.81 \pm 0.05$ . **f** Critical value of the Binder cumulant at the bicritical point,  $U_c$  (black circles), shown as a function of the spin anisotropy. For comparison we show  $U_c$  values at the critical points of the Ashkin-Teller model (ATM, red circles). The magenta line is a linear fit which shows that extrapolating  $U_c$  to the spin-isotropic limit ( $\Delta = 1$ ) gives good agreement with the critical value obtained at  $K/J = 1$  in the ATM, where this model has 4-state Potts universality.

line of (multi)critical points (Fig. 1e); in Sec. S2 of the SI we show further data illustrating this situation in the DTAF phase.

Given the qLRO of the DTAF phase below  $t_{KT}$ , and the LRO of the TC phase below a transition that also appears to converge on the critical line, the crucial question arises of how these field-induced phases affect the universality. We preface the discussion to follow with an important remark: we have found in Figs. 4a-c that all the transition and crossover lines meet with an accuracy of 0.01 in our units, as we show in Sec. S2 of the SI.<sup>34</sup> Rather than perform extensive numerical calculations to achieve a higher accuracy, which still would not serve as a proof of exact convergence, we base our discussions, particularly of the multicritical DTAF-TC point, on the analysis of additional symmetries and related models below. At zero field (Fig. 4a), where neither the DS nor the DTAF possesses finite- $t$  order due to symmetry-breaking, using  $n_t$  as an effective order parameter reveals a liquid-gas-type transition,<sup>16</sup> where the first-order line is terminated by a

critical point with Ising universality, and crossover lines (determined from the specific-heat peaks, Sec. S2 of the SI<sup>34</sup>) appear on both sides of the transition.<sup>18</sup>

At a fixed low field, where the DTAF has a BKT transition that meets the first-order line at the critical point (Fig. 4b), we investigate the nature of criticality by computing the specific heat as a function of system size, as shown in Fig. 4d. The progressive sharpening of the peak can be characterized by its height,  $C_{\max}(L)$ , which in the inset we find follows precisely the  $\ln L$  scaling of Ising universality.<sup>16</sup> Thus we conclude that the BKT transition has no effect on the universality of the critical point in this instance, and we explain this result below.

Turning now to the DTAF-TC transition, in Fig. 4c we show the situation at  $h = 6$  and in Sec. S2 of the SI<sup>34</sup> we present results elsewhere on this phase boundary. Figure 4e shows explicitly how the discontinuity in the TC order parameter at  $t < t_c$  becomes smooth at and above  $t_c = 0.31$ . At minimum (neglecting the BKT transition), the merging of the discontinuous DTAF-TC line

with the continuous thermal transition of the TC phase should change the Ising critical point to a tricritical Ising point. To determine how the universality is altered, in Fig. 4f we consider the scaling collapse of all our finite- $L$  data at  $t_c$  for  $h = 6$  and extract the critical exponents  $\nu = 0.67 \pm 0.03$  and  $\beta = 0.083 \pm 0.005$ . These values are far from the Ising and tricritical Ising cases, instead corresponding very well to 4-state Potts universality, where  $\nu = 2/3$  and  $\beta = 1/12$ .<sup>40</sup>

*A priori*, this Potts criticality comes as a complete surprise, because the FFB model in a field has no  $S_4$  permutation symmetry, and thus it satisfies all the criteria of an emergent phenomenon. Our discovery of such an exact 4-state Potts universality also appears highly unlikely if the meeting of the three transition lines at a single multicritical point were not exact. To gain further insight, we follow a series of mappings to unveil the underlying symmetries of the system, and summarize the procedure here (a more complete discussion is presented in Sec. S3 of the SI<sup>34</sup>). First we map the quantum model of Eq. (2) to a classical model consisting of an  $O(3)$  rotor, representing the spin degrees of freedom, coupled to an Ising variable representing the triplon density. It is easy to perform large-scale Monte Carlo simulations of this model, and in Fig. 5a we show that the phase diagram at  $h = 6$  is very similar, even semi-quantitatively, to the quantum one (Fig. 4c). A BKT transition arises for the rotors in an applied field and a density-driven Ising transition breaks the sublattice symmetry. Across the critical point where the BKT and Ising transitions meet, we again find  $\nu \simeq 2/3$  and  $\beta \simeq 1/12$ , meaning that the classical model also has 4-state Potts universality.

Next we introduce an Ising-type spin anisotropy,  $\Delta > 1$ , that breaks the  $U(1)$  spin symmetry to  $Z_2$ , turning the BKT transition into a thermal Ising transition, below which the system has true LRO that we denote as “x-Ising” in Fig. 5b. In this situation, the two Ising transitions meet at a bicritical point, below which the transition directly from x-Ising to TC is first-order. The bicritical scenario provides a well accepted instance where the three transition lines do meet at a single point, as our numerical results indicate for the FFB model (Fig. 4c). The correlation-length exponent,  $\nu$ , that we obtain from scaling collapse at the bicritical point varies between  $2/3$  and  $1$  with the strength of spin anisotropy, as we show in Sec. S3 of the SI<sup>34</sup>, and thus the anisotropic classical model has non-universal behaviour.

Because both the DTAF and TC phases break the sublattice symmetry, each has two degenerate configurations,<sup>41</sup> and in total four ground-state configurations are degenerate at the transition. Here the triplon density drops from  $n_t = 1$  in the DTAF to  $n_t = 1/2$  in the TC, and the evolution of  $n_t$  with  $J$  across the emerging critical point indicates a particle-hole symmetry about  $n_t = 3/4$  (Fig. 5c). Defining the Ising variables  $\sigma_i$ , associated with the sublattice symmetry, and  $\eta_i$ , associated with the particle-hole symmetry, the Ising variable  $\tau_i = \sigma_i \eta_i$  obeys the relations  $\tau \rightarrow -\sigma$  and  $\sigma \rightarrow -\tau$  un-

der spin inversion. With these variables we construct the minimal effective model that should describe the critical properties around the emerging critical point in the form

$$H_{\text{eff}} = -J \sum_{i,j} (\sigma_i \sigma_j + \tau_i \tau_j) - K \sum_{i,j} (\sigma_i \sigma_j)(\tau_i \tau_j), \quad (3)$$

as discussed in detail in Sec. S3 of the SI.<sup>34</sup> This model is precisely the Ashkin-Teller model (ATM). It is well known<sup>42</sup> that the ATM exhibits non-universal exponents, which lie between Ising and Potts universalities, along the critical line obtained for  $0 \leq K/J \leq 1$ .

To analyse the correspondence between this ATM and the classical model with variable spin anisotropy, we define a composite order parameter,  $O_b^2 = O_x^2 + O_{\text{TC}}^2$ , that contains the order of both the x-Ising and TC phases (Sec. S3C of the SI<sup>34</sup>). We then consider the Binder cumulant associated with  $O_b$ ,  $U = 2(1 - \langle O_b^4 \rangle / 2 \langle O_b^2 \rangle^2)$ , which has the property that  $U \rightarrow 1$  deep in both ordered phases, but dips across the bicritical point. Figure 5d shows this evolution of  $U$  for a range of system sizes, from whose touching point we determine both the location of the bicritical point and the value  $U_c$ . Because of its dimensionless nature,  $U_c$  should also reflect the universality of the critical point,<sup>43–46</sup> and the scaling collapse shown in Fig. 5e presents an accurate means of extracting  $\nu$ . For the spin-anisotropic model, we find that both  $U_c$  and  $\nu$  vary with the anisotropy  $\Delta$ , exhibiting a non-universal evolution such that  $\nu$  at the bicritical point varies between  $1$  and  $2/3$ , signalling a continuous change between Ising and 4-state Potts universality. The monotonic dependence of  $U_c$  on  $\Delta$ , shown in Fig. 5f, compares exactly with the  $K/J$  scaling of the ATM, and its extrapolated value as  $\Delta \rightarrow 1$  agrees well with the value  $U_c \rightarrow 0.792 \pm 0.003$  found for the ATM at the Potts point.<sup>46</sup>

## Discussion

We have presented the global phase diagram of the FFB Heisenberg model in an applied magnetic field, showing how the field allows systematic control over the phase competition. We have explained the rich variety of phase transitions and (multi)critical lines or points, and found numerical evidence for a striking example of emerging critical behaviour. This emergent 4-state Potts universality, arising along the line of multicritical points where the BKT transition of the DTAF and the Ising one of the TC phase meet, implies that the multicritical system has a higher  $S_4$  permutation symmetry that the microscopic spin model does not possess. This result is clearly different from previous studies of transitions between BKT and Ising phases, such as the well known FFX [U(1)  $\otimes$  Z<sub>2</sub>] model,<sup>47</sup> of anisotropic Heisenberg spin models<sup>48</sup> and of higher symmetries emerging from combined Ising order parameters.<sup>12,13</sup> In the FFB, a symmetry analysis reveals an additional particle-hole symmetry that lies beyond all of these models and can be used to map the critical system to an effective ATM. The generic ATM has a wide parameter regime where

one line of critical points has nonuniversal and continuously varying exponents, as we find in the model with spin anisotropy. In the isotropic limit, where the spin symmetry is enhanced to  $U(1)$ , we expect 4-state Potts universality (i.e. an enhanced  $S_4$  symmetry), because the Potts point is the only multicritical point with enhanced symmetry in the ATM.<sup>49</sup> Precisely how this effective  $S_4$  symmetry emerges in the critical behaviour as the spin symmetry is restored to  $U(1)$  is a well defined problem that deserves further exploration in the expanding field of emergent phenomena.

We found at low fields that the BKT phase of the DTAF has no effect on the Ising nature of the zero-field critical point. This result is explained by the fact that the phase mode associated with the BKT transition couples only marginally to the Ising variable (the triplet density, which is an amplitude mode), as we discuss in Sec. S3 of the SI.<sup>34</sup> At fields high enough to create the TC phase, the BKT nature of the DTAF again plays no role in determining the properties, including the emergent Potts universality, of the multicritical line: our construction of the ATM relied on the symmetries of the system, but not on the presence of qLRO when the spin anisotropy is removed. The origin of this result may be traced by considering the conformally invariant field theories (CFTs) describing the criticality in two-dimensional systems.<sup>50</sup> The ATM with  $K \leq J$  is described by a  $c = 1$  CFT. The BKT transition also has  $c = 1$ , and hence its action on the ATM is only marginal, with the result that the universality class is not altered.

We expect that the multicritical points, emergent critical properties and QCEP we find in the FFB model are directly relevant to a number of dimerized and frustrated quantum magnetic materials. The magnetic properties of  $Ba_2CoSi_2O_6Cl_2$  were suggested to be those of the FFB model with an in-plane spin anisotropy,<sup>51</sup> and one might anticipate exploring some of the FFB phase diagram under combined field and pressure. The zero-field Ising critical point of the FFB has been found in  $SrCu_2(BO_3)_2$ ,<sup>21</sup> and our results for the TC phase boundaries should help to interpret the transitions to the plaquette phase of this system (both have broken  $Z_2$  symmetry).  $SrCu_2(BO_3)_2$  exhibits a cascade of fractional magnetization plateau states at higher applied fields,<sup>24</sup> and at higher pressures has the plaquette and AF phases of the SSM,<sup>14</sup> raising the prospect of multiple opportunities to search for emergent critical behaviour along the associated phase-transition lines.<sup>52</sup> Thus we expect our results to provide a useful foundation for new theoretical and experimental studies of criticality and emergent phenomena.

## Methods

We study the quantum phase diagram of the FFB model using the PESS tensor-network method.<sup>30</sup> The simplex basis allows a highly efficient encoding of the entanglement in frustrated quantum spin systems, and its construction is described in Sec. S1 of the SI.<sup>34</sup> The lattice translation symmetry is used to work on a spa-

tially infinite system and the ground state is found by evolution in imaginary time, for which a simple-update method is sufficient in the FFB. Because three of the four ground states are known exactly, detailed calculations pushing the limits of the truncation parameter ( $D$ , the tensor bond dimension) are not required to achieve accurate convergence (Sec. S1).

As noted above, the total absence of a sign problem in the fully frustrated model ( $J_{\parallel} = J_{\times}$ ) makes SSE QMC simulations possible on large systems and at low temperatures. To extract the maximum accuracy from our simulations, in particular for the determination of critical points and exponents, we exploit the finite-size scaling properties of the known phases.

The transition to the TC phase is studied by defining the dimer-triplet correlation function

$$R(\vec{k}) = L^{-2} \sum_{ij} e^{i\vec{k} \cdot (\vec{r}_i - \vec{r}_j)} \langle (T_i^2 - 1)(T_j^2 - 1) \rangle, \quad (4)$$

from which we obtain the correlation length

$$\xi = \frac{2\pi}{L} \sqrt{R(\vec{Q})/R(\vec{Q} + \delta\vec{Q}) - 1} \quad (5)$$

and the order parameter

$$O^2 = R(\vec{Q})/L^2, \quad (6)$$

where  $\vec{Q} = (\pi, \pi)$  is the ordering wavevector and  $\delta\vec{Q} = (2\pi/L, 0)$ . We obtain the critical exponents by establishing the scaling collapse of both quantities in the forms<sup>39</sup>

$$\begin{aligned} \xi &= LF_{\xi,g}(|g|L^{1/\nu}), \\ O^2 &= L^{2\beta/\nu} F_{O,g}(|g|L^{1/\nu}), \end{aligned} \quad (7)$$

where  $|g|$  denotes the three quantities  $|J - J_c|$ ,  $|h - h_c|$  and  $|t - t_c|$  that we use to effect a systematic approach to the critical points when the other variables are fixed to their critical values.  $F$  denotes a single function that describes all the data when scaled in this way, allowing a highly accurate determination of the critical exponents.

To study the BKT transition, we calculate the spin stiffness from the expression  $\rho_s = \frac{1}{2}t\langle w_x^2 + w_y^2 \rangle$ , in which  $w_\alpha = \sum_b (N_{b,\alpha}^+ - N_{b,\alpha}^-)/L$  with  $\alpha$  denoting the direction  $x$  or  $y$  and  $N_{b,\alpha}^\pm$  expressing the number of operators  $T_{i(b)}^\pm T_{j(b)}^\mp$  associated with bond  $b$  in direction  $\alpha$  appearing in the QMC operator sequence.<sup>39</sup> The system size can again be used to effect a scaling collapse of  $\rho_s$  to the form employed in Fig. 3,<sup>38,39</sup>

$$\rho_s = \frac{2t_{KT}}{\pi} \left[ 1 + \frac{1}{2 \ln L + c} \right] F_\rho(\ln L - a/\sqrt{t - t_{KT}}), \quad (9)$$

where  $a$  and  $c$  are fitting parameters and  $F_\rho(t, L)$  is a single scaling function. This collapse allows an accurate determination of the BKT transition temperature,  $t_{KT}$ .



- [1] Zinn-Justin, J. *Quantum Field Theory and Critical Phenomena* (Oxford University Press, Oxford, 2002).
- [2] Savary, L. & Balents, L. Quantum spin liquids: a review. *Rep. Prog. Phys.* **80**, 016502 (2017).
- [3] Sachdev, S. *Quantum Phase Transitions, Second Edition* (Cambridge University Press, Cambridge, 2011).
- [4] Zapf, V., Jaime, M. & Batista, C. Bose-Einstein condensation in quantum magnets. *Rev. Mod. Phys.* **86**, 563 (2014).
- [5] Merchant, P. *et al.* Quantum and classical criticality in a dimerized quantum antiferromagnet. *Nature Phys.* **10**, 373–379 (2014).
- [6] Senthil, T., Vishwanath, A., Balents, L., Sachdev, S. & Fisher, M. P. A. Deconfined Quantum Critical Points. *Science* **303**, 1490–1494 (2004).
- [7] Senthil, T., Balents, L., Sachdev, S., Vishwanath, A. & Fisher, M. P. A. Quantum criticality beyond the Landau-Ginzburg-Wilson paradigm. *Phys. Rev. B* **70**, 144407 (2004).
- [8] Zhao, B., Takahashi, J. & Sandvik, A. W. Multicritical Deconfined Quantum Criticality and Lifshitz Point of a Helical Valence-Bond Phase. *Phys. Rev. Lett.* **125**, 257204 (2020).
- [9] Lu, D.-C., Xu, C. & You, Y.-Z. Self-duality protected multi-criticality in deconfined quantum phase transitions. *Phys. Rev. B* **104**, 205142 (2021).
- [10] Shao, H., Guo, W. & Sandvik, A. W. Quantum criticality with two length scales. *Science* **352**, 213–216 (2016).
- [11] Zhao, B., Weinberg, P. & Sandvik, A. Symmetry-enhanced discontinuous phase transition in a two-dimensional quantum magnet. *Nat. Phys.* **15**, 678 (2019).
- [12] Zhu, G.-Y. & Zhang, G.-M. Gapless Coulomb State Emerging from a Self-Dual Topological Tensor-Network State. *Phys. Rev. Lett.* **122**, 176401 (2019).
- [13] Schuler, M., Henry, L.-P., Lu, Y.-M. & Läuchli, A. M. Emergent XY\* transition driven by symmetry fractionalization and anyon condensation. *SciPost Phys.* **14**, 001 (2023).
- [14] Zayed, M. *et al.* 4-spin plaquette singlet state in the Shastry-Sutherland compound  $\text{SrCu}_2(\text{BO}_3)_2$ . *Nat. Phys.* **13**, 962 (2017).
- [15] Yu, R. *et al.* Bose glass and Mott glass of quasiparticles in a doped quantum magnet. *Nature* **489**, 379 (2012).
- [16] Stapmanns, J. *et al.* Thermal Critical Points and Quantum Critical End Point in the Frustrated Bilayer Heisenberg Antiferromagnet. *Phys. Rev. Lett.* **121**, 127201 (2018).
- [17] Chaikin, P. M. & Lubensky, T. C. *Principles of Condensed Matter Physics* (Cambridge University Press, Cambridge, 1995).
- [18] Weber, L. *et al.* Quantum Monte Carlo simulations in the trimer basis: first-order transitions and thermal critical points in frustrated trilayer magnets. *SciPost Phys.* **12**, 054 (2022).
- [19] Weber, L., Fache, A. Y. D., Mila, F. & Wessel, S. Thermal critical points from competing singlet formations in fully frustrated bilayer antiferromagnets. *Phys. Rev. B* **106**, 235128 (2022).
- [20] Strečka, J. *et al.* Thermal first-order phase transitions, Ising critical points, and reentrance in the Ising-Heisenberg model on the diamond-decorated square lattice in a magnetic field. *Phys. Rev. B* **107**, 134402 (2023).
- [21] Larrea Jiménez, J. *et al.* A quantum magnetic analogue to the critical point of water. *Nature* **592**, 370 (2021).
- [22] Shastry, B. S. & Sutherland, B. Exact ground state of a quantum mechanical antiferromagnet. *Physica B+C* **108**, 1069–1070 (1981).
- [23] Kageyama, H. *et al.* Exact Dimer Ground State and Quantized Magnetization Plateaus in the Two-Dimensional Spin System  $\text{SrCu}_2(\text{BO}_3)_2$ . *Phys. Rev. Lett.* **82**, 3168 (1999).
- [24] Matsuda, Y. H. *et al.* Magnetization of  $\text{SrCu}_2(\text{BO}_3)_2$  in Ultrahigh Magnetic Fields up to 118 T. *Phys. Rev. Lett.* **111**, 137204 (2013).
- [25] Lee, J. Y., You, Y.-Z., Sachdev, S. & Vishwanath, A. Signatures of a Deconfined Phase Transition on the Shastry-Sutherland Lattice: Applications to Quantum Critical  $\text{SrCu}_2(\text{BO}_3)_2$ . *Phys. Rev. X* **9**, 041037 (2019).
- [26] Cui, Y. *et al.* Proximate deconfined quantum critical point in  $\text{SrCu}_2(\text{BO}_3)_2$ . *Science* **380**, 1179–1184 (2023).
- [27] Alet, F., Damle, K. & Pujari, S. Sign-Problem-Free Monte Carlo Simulation of Certain Frustrated Quantum Magnets. *Phys. Rev. Lett.* **117**, 197203 (2016).
- [28] Honecker, A. *et al.* Thermodynamic properties of highly frustrated quantum spin ladders: Influence of many-particle bound states. *Phys. Rev. B* **93**, 054408 (2016).
- [29] Syljuåsen, O. F. & Sandvik, A. W. Quantum Monte Carlo with directed loops. *Phys. Rev. E* **66**, 046701 (2002).
- [30] Xie, Z. Y. *et al.* Tensor Renormalization of Quantum Many-Body Systems Using Projected Entangled Simplex States. *Phys. Rev. X* **4**, 011025 (2014).
- [31] Richter, J., Derzhko, O. & Krokhnalskii, T. Finite-temperature order-disorder phase transition in a frustrated bilayer quantum Heisenberg antiferromagnet in strong magnetic fields. *Phys. Rev. B* **74**, 144430 (2006).
- [32] Derzhko, O., Krokhnalskii, T. & Richter, J. Emergent Ising degrees of freedom in frustrated two-leg ladder and bilayer  $s = \frac{1}{2}$  Heisenberg antiferromagnets. *Phys. Rev. B* **82**, 214412 (2010).
- [33] Richter, J., Krupnitska, O., Baliha, V., Krokhnalskii, T. & Derzhko, O. Thermodynamic properties of  $\text{Ba}_2\text{CoSi}_2\text{O}_6\text{Cl}_2$  in a strong magnetic field: Realization of flat-band physics in a highly frustrated quantum magnet. *Phys. Rev. B* **97**, 024405 (2018).
- [34] The Supplementary Information at <http://xxx.yyy.zzz> contains extended information concerning our iPESS calculations, QMC simulations and data analysis, further figures adding information about (emergent) criticality in the FFB and full discussions of the classical model, spin-anisotropic model and Ashkin-Teller Model to which we appeal in our analysis.
- [35] Fisher, M. E. & Upton, P. J. Universality and interfaces at critical end points. *Phys. Rev. Lett.* **65**, 2402 (1990).
- [36] Berezinskii, V. L. Destruction of Long-range Order in One-dimensional and Two-dimensional Systems Possessing a Continuous Symmetry Group. II. Quantum Systems. *Sov. Phys. JETP* **34**, 610 (1972).
- [37] Kosterlitz, J. M. & Thouless, D. J. Long range order and metastability in two dimensional solids and superfluids. (Application of dislocation theory). *J. Phys. C: Solid State Phys.* **5**, L124 (1972).

- [38] Weber, H. & Minnhagen, P. Monte Carlo determination of the critical temperature for the two-dimensional XY model. *Phys. Rev. B* **37**, 5986 (1988).
- [39] Sandvik, A. W. Computational Studies of Quantum Spin Systems. *AIP Conf. Proc.* **1297**, 135–338 (2010).
- [40] Wu, F. Y. The Potts model. *Rev. Mod. Phys.* **54**, 235 (1982).
- [41] The DTAF breaks a continuous U(1) symmetry, but retains a double degeneracy when the orientation of the staggered order parameter is defined. One configuration is illustrated in Fig. 1b and the other can be obtained by exchanging both spins on alternating sites of the square lattice (i.e. by a sublattice transformation).
- [42] Wiseman, S. & Domany, E. Cluster method for the Ashkin-Teller model. *Phys. Rev. E* **48**, 4080 (1993).
- [43] Goldenfeld, N. *Lectures on Phase Transitions and the Renormalization Group* (Addison-Wesley, Reading, 1992).
- [44] Chen, X. S. & Dohm, V. Nonuniversal finite-size scaling in anisotropic systems. *Phys. Rev. E* **70**, 056136 (2004).
- [45] Selke, W. & Shchur, L. N. Critical Binder cumulant in two-dimensional anisotropic Ising models. *J. Phys. A* **38**, L739 (2005).
- [46] Jin, S., Sen, A. & Sandvik, A. W. Ashkin-Teller Criticality and Pseudo-First-Order Behavior in a Frustrated Ising Model on the Square Lattice. *Phys. Rev. Lett.* **108**, 045702 (2012).
- [47] Song, F.-F. & Zhang, G.-M. Tensor network approach to the two-dimensional fully frustrated XY model and a chiral ordered phase. *Phys. Rev. B* **105**, 134516 (2022). and references therein.
- [48] Holtschneider, M., Wessel, S. & Selke, W. Classical and quantum two-dimensional anisotropic Heisenberg antiferromagnets. *Phys. Rev. B* **75**, 224417 (2007).
- [49] Dijkgraaf, R., Verlinde, E. & Verlinde, H.  $c = 1$  conformal field theories on Riemann surfaces. *Commun. Math. Phys.* **115**, 649–690 (1988).
- [50] Friedan, D., Qiu, Z. & Shenker, S. Conformal Invariance, Unitarity, and Critical Exponents in Two Dimensions. *Phys. Rev. Lett.* **52**, 1575 (1984).
- [51] Tanaka, H. *et al.* Almost Perfect Frustration in the Dimer Magnet Ba<sub>2</sub>CoSi<sub>2</sub>O<sub>6</sub>Cl<sub>2</sub>. *J. Phys. Soc. Jpn.* **83**, 103701 (2014).
- [52] Shi, Z. *et al.* Discovery of quantum phases in the Shastry-Sutherland compound SrCu<sub>2</sub>(BO<sub>3</sub>)<sub>2</sub> under extreme conditions of field and pressure. *Nature Commun.* **13**, 2301 (2022).
- [53] Liao, H. J. *et al.* Gapless Spin-Liquid Ground State in the  $S = 1/2$  Kagome Antiferromagnet. *Phys. Rev. Lett.* **118**, 137202 (2017).
- [54] Jiang, H. C., Weng, Z. Y. & Xiang, T. Accurate Determination of Tensor Network State of Quantum Lattice Models in Two Dimensions. *Phys. Rev. Lett.* **101**, 090603 (2008).
- [55] Phien, H. N., Bengua, J. A., Tuan, H. D., Corboz, P. & Orús, R. Infinite projected entangled pair states algorithm improved: Fast full update and gauge fixing. *Phys. Rev. B* **92**, 035142 (2015).
- [56] Wang, L. & Verstraete, F. Cluster update for tensor network states. *arXiv:1110.4362* (2011).
- [57] Corboz, P., Rice, T. M. & Troyer, M. Competing States in the  $t$ - $J$  Model: Uniform  $d$ -Wave State versus Stripe State. *Phys. Rev. Lett.* **113**, 046402 (2014).
- [58] Selke, W. Critical Binder cumulant of two-dimensional Ising models. *Eur. Phys. J. B* **51**, 223 (2006).
- [59] Jin, S., Sen, A., Guo, W. & Sandvik, A. W. Phase transitions in the frustrated Ising model on the square lattice. *Phys. Rev. B* **87**, 144406 (2013).
- [60] Cristofano, G., Marotta, V., Minnhagen, P., Naddeo, A. & Niccoli, G. CFT description of the fully frustrated XY model and phase diagram analysis. *J. Stat. Mech. Theory Exp.* **2006**, P11009 (2006).

**Data availability** The data that support the findings of this study are available from the corresponding author upon reasonable request.

**Code availability** The code that supports the findings of this study is available from the corresponding author upon reasonable request.

#### Acknowledgements

We thank F. Mila, Y. Wan, Y. Wang, S. Wessel and W. Yu for helpful discussions. This work was supported in part by the National Natural Science Foundation of China under Grant Nos. 11974396, 12174441 and 12188101. We acknowledge the Physical Laboratory of High-Performance Computing at Renmin University of China for the provision of computational resources and the National Supercomputer Center in Guangzhou for the use of the Tianhe-2 supercomputer.

#### Author contributions

The project was conceived by B.N. and R.Y. QMC calculations were performed by Y.F. and PESS calculations by N.X. Theoretical interpretation was provided by Y.F., C.L., B.N. and R.Y. The manuscript was written by Y.F., B.N. and R.Y. with contributions from all the authors.

**Competing financial interests** The authors declare no competing financial interests.

#### Additional information

**Supplementary information** The online version contains supplementary material available at <https://doi.org/xxx.yyy.zzz>.

**Correspondence and requests for materials** should be addressed to B.N. and R.Y.

## Supplementary information to accompany the article

### “Emergent criticality in fully frustrated quantum magnets”

Yuchen Fan, Ning Xi, Changle Liu, Bruce Normand and Rong Yu

#### S1. TENSOR-NETWORK RESULTS FOR THE GROUND STATES OF THE QUANTUM MODEL

We determine the  $t = 0$  phase diagram of the fully frustrated bilayer (FFB) model, shown in Fig. 1c of the main text, by applying the tensor-network method of infinite projected entangled simplex states (iPESS).<sup>30</sup> In this construction, illustrated in Fig. S1a, a projection tensor,  $U$ , is defined on each site of a square lattice, which contains the two spins of the inter-layer dimer. Four  $U$  tensors around a single square are connected by simplex tensors,  $S$ , which reside at the centres of alternating squares.

The  $S$  tensors do not carry any physical spin degrees of freedom, but are introduced to allow an optimal account of the spin entanglement. It has been shown that this construction delivers an excellent description of the ground states of a number of frustrated spin systems.<sup>30,53</sup> iPESS calculations are performed for an infinitely large system by employing the translational symmetry. For the FFB we take a  $2 \times 2$  unit cell containing two independent  $S$  tensors and four  $U$  tensors.

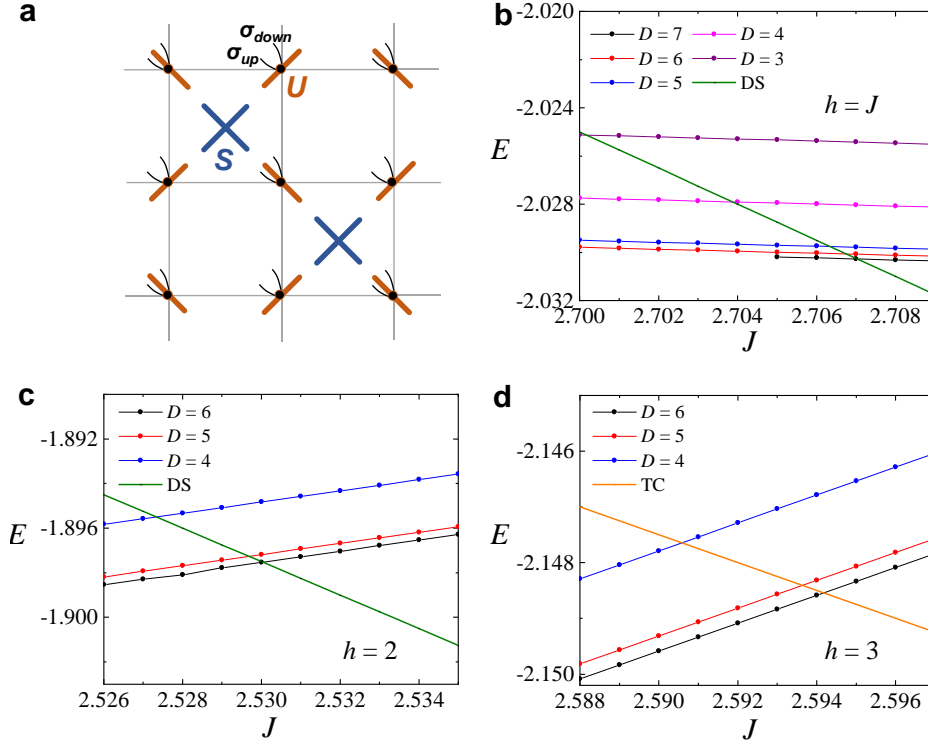


FIG. S1. **Tensor-network calculations.** **a** iPESS framework for bilayer computations. A simplex  $S$  tensor (blue) is placed at the centres of alternating squares on a square lattice, and is connected to four  $U$  tensors (red) placed on the lattice sites. Each  $U$  tensor encodes the two physical  $S = 1/2$  spins of the bilayer dimer unit and two auxiliary variables, while each  $S$  tensor encodes four auxiliary variables. Each tensor has bond dimension  $D$ , which is the truncation parameter of the calculation. To draw the quantum phase diagram shown in Fig. 1c of the main text, iPESS is required only to compute the energy of the DTAF phase, which is then compared with the exactly known energies of the DS, TC and FM phases. **b** Comparison of energies in the vicinity of first-order transitions between the DTAF phase (lines with symbols) and the DS phase (solid green line) at  $h = 2$ . **c** Comparison of energies between the DTAF phase and the TC phase (solid orange line) at  $h = 3$ . **d** Comparison of energies between the DTAF phase and the degenerate DS and TC phases (solid green line) at  $h = J$ , shown around their triple point.

To determine the ground states, we start from a random initial state and perform imaginary-time evolution<sup>30,54–56</sup> by the simple-update method.<sup>30,54</sup> After convergence of the state has been achieved, we use the

corner-transfer-matrix renormalization-group (CTMRG) method<sup>57</sup> to contract the infinite network and calculate the expectation values of physical observables. In certain parameter regimes, more than one converged state can

be stabilized when starting from different initial states, and in this case the ground state is selected by comparing energies. From this procedure we identify four ground states, the dimer singlet (DS), triplon crystal (TC), dimer triplet antiferromagnetic (DTAF) and ferromagnetic (FM) states. The DS, TC and FM states are all product states, which are easily constructed in the basis of interlayer dimers as

$$|\text{DS}\rangle = \prod_{i=1}^N |S\rangle_i, \quad (\text{S1})$$

$$|\text{TC}\rangle = \prod_{i \in A, j \in B} |S\rangle_i |T_{+1}\rangle_j, \quad (\text{S2})$$

$$|\text{FM}\rangle = \prod_{i=1}^N |T_z\rangle_i, \quad (\text{S3})$$

where

$$|S\rangle = \frac{1}{\sqrt{2}} |\uparrow_1 \downarrow_2 - \downarrow_1 \uparrow_2\rangle \quad \text{and} \quad (\text{S4})$$

$$|T_{+1}\rangle = |\uparrow_1 \uparrow_2\rangle \quad (\text{S5})$$

are dimer singlet and triplet states defined on one site of the square lattice. The energies of these states are readily obtained analytically as

$$E_{\text{DS}} = -\frac{3}{4}J, \quad (\text{S6})$$

$$E_{\text{TC}} = -\frac{1}{4}J - \frac{1}{2}h \quad \text{and} \quad (\text{S7})$$

$$E_{\text{FM}} = \frac{1}{4}J - h \quad (\text{S8})$$

per dimer. These product states can all be expressed as tensor-network states with bond dimension  $D = 1$ , and the energies calculated numerically in the iPESS representation match exactly with the analytical results.

A determination of the phase boundaries therefore requires only a comparison of the calculated energy for the DTAF state with those of the other three states. Results in three representative parameter regimes are shown in Fig. S1. In each case, we find rapid convergence of the DTAF energy with increasing  $D$ , even at very moderate  $D$  values, and thus it is not necessary to push our calculations to large  $D$ . Figures S1b and S1c show respectively the extraction of phase-boundary points for the DS-DTAF and TC-DTAF transitions. The DS-TC transition occurs along the line  $h = J$ , where the two states are degenerate with energy  $E = -\frac{3}{4}J$  per dimer, and the crossing point of the DTAF and DS/TC energies along this trajectory determines the triple point. Once again, the energy of the DTAF state converges rapidly with increasing  $D$ , and the triple point can be located accurately at  $J = 2.707 \pm 0.001$  (using  $D = 7$ ). Thus we find that our tensor-network calculations deliver precise phase boundaries for the FFB model, with numerical error bars arising from the finite  $D$  or other parts of the optimization process being smaller than the symbol sizes in the phase diagram shown in Fig. 1c of the main text.

## S2. THERMAL PHASE TRANSITIONS AND CRITICAL BEHAVIOUR OF THE QUANTUM MODEL

The FFB model in a field possesses a rich phase diagram at finite temperatures, as Fig. 1e of the main text

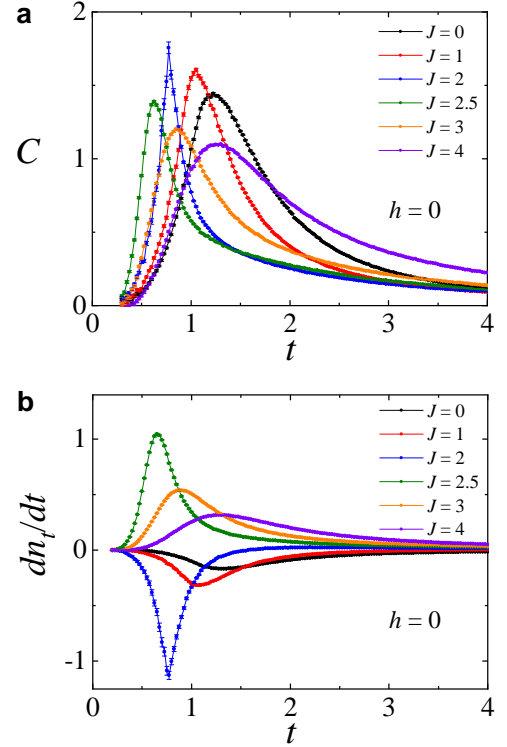


FIG. S2. **Zero-field physics.** **a** Specific heat,  $C$ , shown as a function of the reduced temperature,  $t$ , at  $h = 0$  for selected values of  $J$ . **b** Temperature derivative of the triplet density,  $dn_t/dt$ , shown as a function of  $t$  for same parameters. In both cases, the peak position marks the characteristic temperature of the crossover to a correlated spin state (shown as the magenta points in Figs. 1e and 2a of the main text). The system size is  $L = 24$ .

makes clear. Although the magnetic long-range order of the DTAF phase cannot persist at finite temperature as a consequence of the Mermin-Wagner theorem, the first-order phase transitions driven by increasing  $J$  do persist. The three ground states appearing below saturation have different triplet densities, with  $n_t = 1$  per dimer site in the DTAF,  $n_t = 1/2$  in the TC and  $n_t = 0$  in the DS phase. At low temperatures,  $n_t$  jumps between different parameter regimes in first-order transitions (shown as the walls of discontinuities in Fig. 1e), but as the temperature increases, the differences in triplet density reduce and eventually vanish. Here the walls of first-order transitions are terminated by a lines of critical points. Our most striking result is how the nature of this critical point depends on the strength of the applied magnetic field: Figs. 4a-c of the main text show the three different scenarios obtained when the three-dimensional (3D) phase diagram is analysed at different field values. The critical behaviour in each regime is discussed in the main text, and here we provide additional data that supplement all of the conclusions drawn there.

**Ising critical point at  $h = 0$ .** The critical point terminating the first-order line at  $h = 0$  has been studied

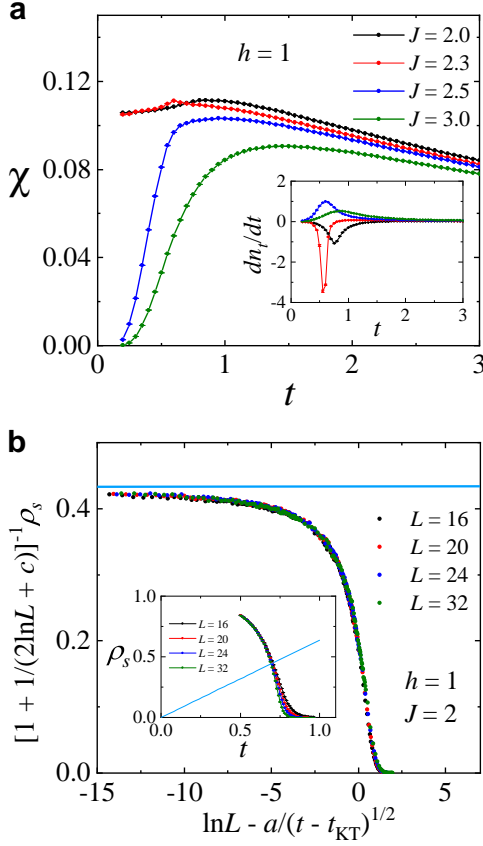


FIG. S3. **Physics of the DTAF.** **a** Uniform susceptibility,  $\chi(t)$ , computed with  $L = 24$  at  $h = 1$  for selected  $J$  values.  $\chi(t)$  converges to a finite value as  $t \rightarrow 0$  in the DTAF phase. The inset allows a comparison of the peaks in  $\chi(t)$  with those in  $C(t)$  and  $dn_t/dt$ , which were used to extract the magenta points shown in Figs. 1e and 4b of the main text. **b** Finite-size scaling of the spin stiffness,  $\rho_s(t)$ , near the BKT transition obtained by fitting to the form of  $\rho_s(t, L)$  given in the Methods section of the main text, from which we determined  $a = 0.8 \pm 0.05$ ,  $c = -2.0 \pm 0.05$  and the BKT transition temperature  $t_{KT} = 0.676 \pm 0.002$ . The inset shows  $\rho_s$  calculated at  $h = 1$  and  $J = 2$  for a range of system sizes, a form in which  $t_{KT}$  is determined from the crossing point of  $\rho_s(t)$  curve with the linear function  $2t/\pi$  (cyan line) in the limit  $L \rightarrow \infty$ .

previously.<sup>16</sup> Here no spontaneous breaking of symmetry takes place and the first-order transition is of the liquid-gas type, with the critical point having Ising universality. The crossover temperatures shown in Fig. 4a of the main text were determined for both the DTAF and DS phases from the positions of the peaks in the specific heat  $C(t)$ , as shown in Fig. S2a. The crossover can also be characterized using the peak in the derivative of the triplet density,  $dn_t/dt$ , shown in Fig. S2b, which reflects the singlet-triplet nature of this transition.

**Ising critical point at low fields.** At any finite field, the DTAF phase has only quasi-long-ranged order (qLRO) at finite temperatures, and one may question how this affects the nature of the critical point terminat-

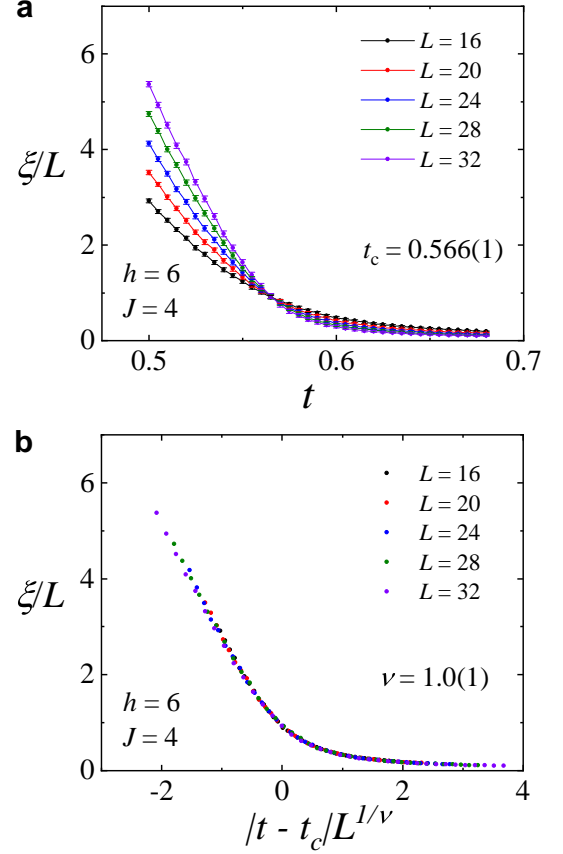


FIG. S4. **Physics of the TC.** **a** Correlation length,  $\xi(t)$ , computed for a range of system sizes in the TC regime ( $J = 4$ ,  $h = 6$ ). The transition temperature,  $t_c = 0.566 \pm 0.001$ , is determined from the crossing point. **b** Scaling collapse of  $\xi(t, L)$ , yielding the critical exponent  $\nu = 1.0 \pm 0.1$ .

ing the DTAF-DS transition. The Berezinskii-Kosterlitz-Thouless (BKT) transition into the qLRO phase does not result in the spontaneous breaking of any symmetry, and the transition temperature,  $t_{KT}$ , does not match with the crossover temperature characterizing the thermodynamic properties, as shown in Fig. 3a of the main text. In Fig. S3a we contrast the susceptibility,  $\chi(t)$ , in the gapped DS phase, where it vanishes as  $t \rightarrow 0$ , with that in DTAF phase, where it approaches a finite value due to the gapless ground state and incipient LRO. In Fig. S3b we examine the BKT transition in more detail for one parameter choice in the low-field regime,  $h = 1$  and  $J = 2$ : as in Figs. 3b and 3c of the main text, which were computed at  $h = 6$ , we use the scaling form given in Eq. (9)<sup>38,39</sup> to determine the transition temperature to high accuracy (here  $t_{KT} = 0.676 \pm 0.002$ ).

At  $h = 1$  we identified the critical point as  $J_c = 2.36 \pm 0.01$  and  $t_c = 0.47 \pm 0.01$ . Here the two crossover lines, the BKT transition line and the first-order singlet-triplet transition line all meet, as shown in Fig. 4b of the main text. As noted there, we have demonstrated this meeting at the 0.01 accuracy level in our simulations; in

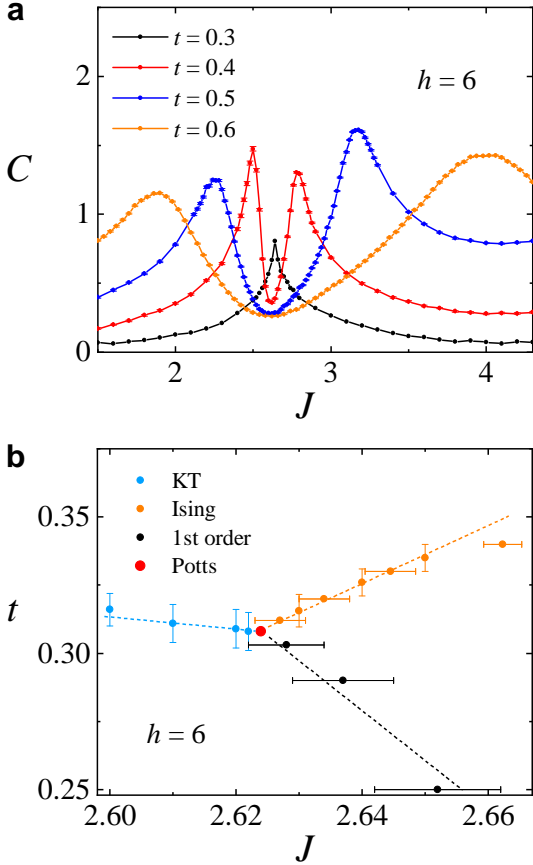


FIG. S5. **Multicritical point.** **a** Specific heat computed at  $L = 24$  and shown as a function of  $J$  at  $h = 6$ . The low- $J$  peaks characterize the crossover on the DTAF side, shown by the magenta points in Figs. 1e and 4c of the main text. The high- $J$  peaks characterize the TC phase. The single peak for  $t < t_c \simeq 0.31$  indicates the DTAF-TC transition. **b** Convergence of first-order and continuous transition lines to a single multicritical point, illustrated for  $h = 6$ . Our calculations indicate convergence to the single point,  $(J_c, t_c) = (2.624(4), 0.308(5))$ , with the accuracy indicated; the maximum system size employed was  $L = 32$ .

fact the exact behaviour of the crossover lines<sup>18</sup> is immaterial for the discussion of criticality, and we found no evidence that the BKT line might not meet the critical point at any  $h$  value. To deduce the universality of this critical line, in Fig. 4d of the main text we showed that the finite-size scaling of the peak value of the specific heat,  $C_{\max} \propto \ln L$ , confirms that the critical point remains of Ising type, meaning that the presence of the qLRO BKT phase does not change the universality from the  $h = 0$  case. In Sec. S3E below we comment in more detail on this result.

#### Emergent critical point at intermediate fields.

When  $h > h_{\text{tr}}$ , the triple point where the DS, TC and DTAF phases meet, the wall of discontinuities separates the DTAF ( $n_t = 1$ ) from the TC ( $n_t = 0.5$ ), where the alternation of dimer singlets and triplets breaks the dis-

crete lattice (translational) symmetry. Thus, as shown in the main text, TC order persists at finite temperatures, exhibiting a continuous thermal transition to the disordered (paramagnetic) phase. In Fig. S4a we show the correlation length,  $\xi(t)$ , calculated for different system sizes at one point in the TC phase ( $h = 6$  and  $J = 4$ ). From the crossing point of the  $\xi(t, L)$  lines we determine the transition temperatures to high accuracy (here  $t_c = 0.566 \pm 0.001$ ). In Fig. S4b we implement the scaling collapse of our finite-size data for  $\xi$  that is analogous to the collapse of the order parameter,  $O$ , of the TC phase (the staggered longitudinal magnetization) shown in Fig. 2c of the main text. Both  $\xi$  and  $O$  confirm that the thermal transition has Ising universality, with critical exponents  $\nu = 1$  and  $\beta = 1/8$ .

In Fig. S5a we use the specific heat at fixed  $h = 6$  to characterize the convergence of the DTAF crossover temperature and the TC transition temperature. Where the two meet as the temperature is reduced marks the critical point, and below this temperature the transition becomes first-order. At the DTAF-TC transition, the issue of the accuracy with which we can demonstrate convergence to one multicritical point becomes important, because even without the crossover lines this point should mark the meeting of one first-order transition line with two well defined lines of continuous transitions (one of which is the KT transition to a qLRO phase). In Fig. S5b we quantify the statement that such a meeting is demonstrated directly at the 0.01 accuracy level. As noted in the main text, our simulations have a finite accuracy and thus cannot demonstrate exact convergence; instead we base our analysis of the multicritical point on (i) the application of symmetry arguments to the equivalent classical model, (ii) its immediate connection to the well accepted bicritical-point scenario if the DTAF phase is given any finite spin anisotropy and (iii) the high precision to which we obtain the scaling exponents of a qualitatively different universality class at the multicritical point estimated to the available precision.

To reiterate the last point, our most remarkable result is the emergent symmetry of the multicritical point (i.e. the point terminating the first-order DTAF-TC transition). As we showed in Fig. 4f of the main text, the scaling of the TC order parameter and the corresponding correlation length through this point give to high accuracy the critical exponents  $\nu = 2/3$  and  $\beta = 1/12$  of 4-state Potts universality.<sup>40</sup> To demonstrate that this universality class is a global property of the full line of emergent critical points, i.e. over the field regime  $h_{\text{tr}} < h < h_{\text{QCEP}}$ , we have calculated the scaling properties at additional field values and in Fig. S6 we show our results for  $h = 5$ .

Figure S6a shows that the fixed-field phase diagram is very similar to the  $h = 6$  case shown in Fig. 4c of the main text. Figure S6b shows the evolution of  $n_t$  as  $J$  is varied at temperatures at and above  $t_c$ . At the critical point,  $n_t = 3/4$ , as also shown in Fig. 4e of the main text. The DTAF and the TC have two different types of order that both break the  $Z_2$  sublattice sym-

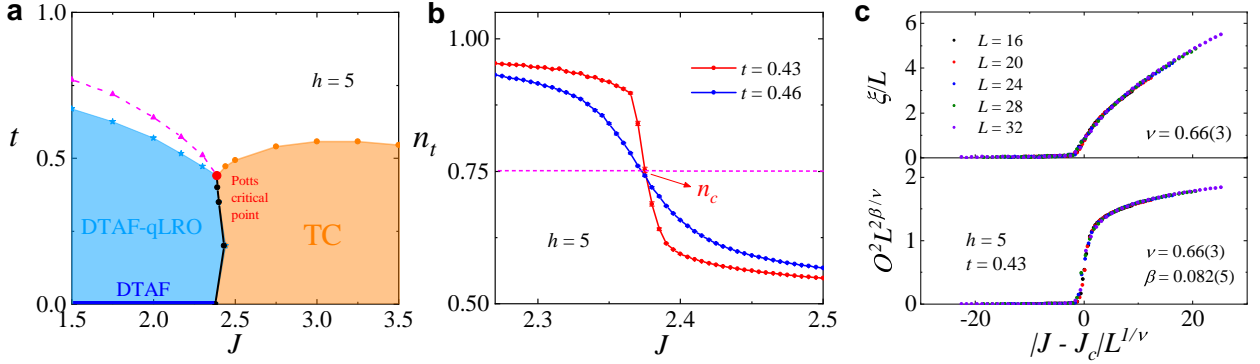


FIG. S6. **Emergent criticality at the DTAF-TC transition.** **a** Phase diagram of the FFB model in the  $J$ - $t$  plane at  $h = 5$ . The phase diagram has the same form as at  $h = 6$  (Fig. 4c of the main text), with the emergent critical point located at  $(J_c, t_c) = (2.378 \pm 0.002, 0.43 \pm 0.01)$ . **b** Triplet density,  $n_t$ , calculated with  $L = 24$  and shown as a function of  $J$  near the emergent critical point, where  $n_t = 0.75$ , indicating a triplet-singlet particle-hole symmetry. **c** Scaling collapse of the correlation length,  $\xi$ , and the order parameter,  $O$ , of the TC phase across the emergent critical point. The critical exponents estimated from these two types of data collapse are  $\nu = 0.66 \pm 0.03$  and  $\beta = 0.082 \pm 0.005$ , fully consistent with 4-state Potts universality.

$\vec{T}$	$ S\rangle$	$ T_{-1}\rangle$	$ T_0\rangle$	$ T_{+1}\rangle$	unphysical	unphysical
$n$	0	1	1	1	0	0
$\mathbf{S}$	$ S^z = 0\rangle$	$ S^z = -1\rangle$	$ S^z = 0\rangle$	$ S^z = 1\rangle$	$ S^z = -1\rangle$	$ S^z = 1\rangle$

TABLE S1. Mapping between the dimer basis (top row) and the slave-spin representation (centre and bottom rows). The unphysical states are eliminated by enforcing a constraint in the slave-spin representation.

metry, giving four ground-state configurations that are degenerate at the  $t = 0$  transition, which has an exact triplet-singlet particle-hole symmetry about  $n_t = 3/4$ . Our results imply that this particle-hole symmetry persists at finite temperature, and indeed up to the emergent critical point. The importance of this symmetry in understanding the nature of the emergent Potts universality is detailed in Sec. S3.

Figure S6c shows the scaling collapse of the correlation length and order parameter, from which we again obtain the critical exponents of the 4-state Potts model to the same precision. We comment that the accuracy of our calculations depends on having a robust  $t_c$ , and thus our error bars become larger as the field is increased well beyond  $h = 6$ , where  $t_c$  decreases monotonically (Fig. 1e of the main text). Again one may ask how this emergent Potts universality arises from the symmetries of the DTAF and TC phases, and whether it is influenced by the BKT physics of the former. Next we study the classical, spin-anisotropic and Ashkin-Teller models offering insight into these questions.

### S3. EMERGENT CRITICALITY IN A CLASSICAL MODEL

#### A. Mapping to a classical model

To better understand the nature of the emergent critical point, and to allow more efficient simulations, we map

the quantum FFB model in the dimer basis [Eq. (2) of the main text] to a classical model defined on the square lattice. We begin by writing

$$\vec{T}_i = n_i \mathbf{S}_i \quad (\text{S9})$$

at each lattice site, where  $n_i = 0$  or 1 is an Ising variable that encodes the triplet density and  $\mathbf{S}_i$  is a slave spin-1 operator. In Table S1 we present the mapping between the local states in the dimer basis and the slave-spin representation, which has an enlarged Hilbert space. The quantum Hamiltonian is then mapped, up to a constant, to

$$H_{\text{cl}} = \sum_{\langle i,j \rangle} n_i n_j \mathbf{S}_i \cdot \mathbf{S}_j + J \sum_i n_i^2 - h \sum_i n_i S_i^z + D \sum_i (1 - n_i) (S_i^z)^2, \quad (\text{S10})$$

where the last term is the constraint. The unphysical states are projected out completely in the limit  $D \rightarrow +\infty$ , but for calculational purposes we employ a soft constraint with  $D \gg J$  and  $h$ .

To study the phase transitions at finite temperatures near the emergent critical point, we make a further approximation by treating  $\mathbf{S}_i$  as a classical  $O(3)$  rotor with unit magnitude. This turns Eq. (S10) into a classical model of Ising variables coupled to  $O(3)$  rotors on the square lattice, with the Zeeman coupling between the magnetic field and the rotor reducing the spin rotational symmetry to an in-plane  $O(2)$ .

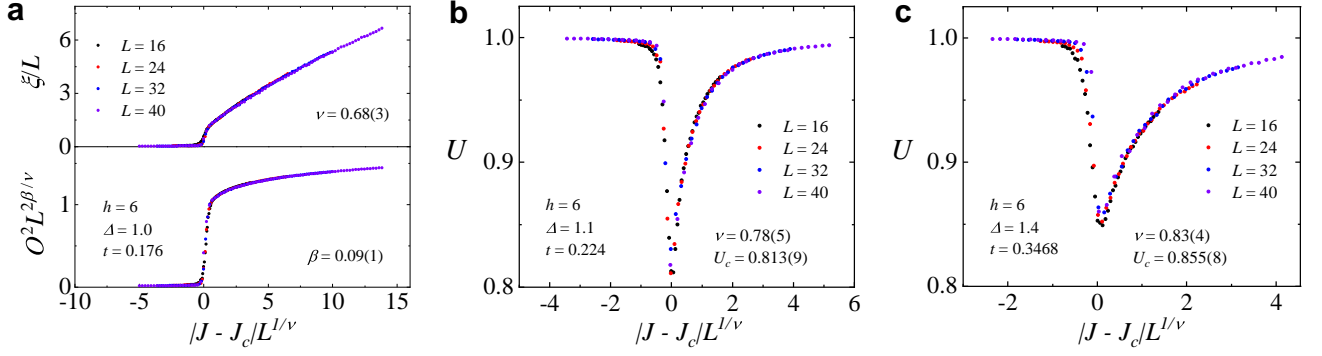


FIG. S7. **Emergent criticality in the classical and spin-anisotropic models.** **a** Scaling collapse of the correlation length and order parameter of the TC phase of the classical model at  $h = 6$ , shown as a function of  $|J - J_c|$  at fixed  $t_c$ . The emergent critical point is located at  $(J_c, t_c) = (1.917 \pm 0.004, 0.176 \pm 0.002)$  and the critical exponents estimated from these two panels are  $\nu = 0.68 \pm 0.03$  and  $\beta = 0.09 \pm 0.01$ . **b** Collapse of Binder-cumulant data shown for the spin-anisotropic model at  $\Delta = 1.1$ . **c** Collapse of Binder-cumulant data shown for the spin-anisotropic model at  $\Delta = 1.4$ .

## B. Phase diagram and emergent criticality

This classical model has a global phase diagram very similar to that of the quantum model, as we showed in Fig. 5a of the main text. Ordering of either the Ising or the rotor variables returns all four phases of the quantum model: the magnetic phases, DTAF and FM, correspond to ordering of the  $O(3)$  rotors, while the DS state has the Ising variable  $n_i = 0$  (singlets) at every site and the TC state is expressed by an alternating order of the Ising variables ( $n_i = 0$  and  $n_i = 1$ ) on the two sublattices. We note that an advantage of this classical model is that it allows the transition to be studied by explicit control of the density ( $n$ ).

Going beyond the phase diagrams (Figs. 4c and 5a of the main text), in Fig. S7a we perform the same scaling-collapse analysis for the correlation length and order parameter of the TC phase that we performed in Fig. 4f of the main text, albeit with larger system sizes. Somewhat remarkably, the critical exponents once again point to emergent 4-state Potts universality in the classical approximation, being entirely consistent with the values  $\nu = 2/3$  and  $\beta = 1/12$ . This property of the classical model allows us to reveal the nature of the critical point by two further pieces of analysis.

## C. Classical model with spin anisotropy

Next we introduce a spin anisotropy in the classical model, so that Eq. (S10) becomes

$$H_{\text{cl}} = \sum_{\langle i,j \rangle} n_i n_j (\Delta S_i^x S_j^x + S_i^y S_j^y + S_i^z S_j^z) + J \sum_i n_i^2 - h \sum_i n_i S_i^z + D \sum_i (1 - n_i) (S_i^z)^2. \quad (\text{S11})$$

For  $\Delta > 1$ , the spin anisotropy is of Ising type and the BKT transition is replaced by an Ising transition into a

phase with long-ranged AF order. The anisotropy has no effect on the TC phase, or on the first-order transition into it, as we showed in the phase diagram of Fig. 5b of the main text. In this model [Eq. (S11)], the critical point where the continuous x-Ising AFM and TC transition lines meet is a conventional bicritical point, below which the direct AFM-TC transition is first-order.

Studying the critical properties of this model is complicated by the fact that both phases have long-range order and both break the same sublattice symmetry. For a reliable analysis we turn to the Binder cumulant,<sup>43–46,58,59</sup> and here we provide full details of the approach summarized in the main text. We define a composite order parameter,  $O_b^2 = O_x^2 + O_{\text{TC}}^2$ , that contains the order of both the AFM and TC phases.

$$O_x = |m_A - m_B|, \text{ with } m_{A/B} = \frac{1}{N} \sum_{i \in A/B} S_i^x / |S_i^x|,$$

is the normalized order parameter of the x-Ising AFM phase and

$$O_{\text{TC}} = |n_A - n_B|, \text{ with } n_{A/B} = \frac{2}{N} \sum_{i \in A/B} n_i,$$

is the order parameter of the TC phase. We then define the Binder cumulant associated with  $O_b$  as

$$U = 2 \left( 1 - \frac{\langle O_b^4 \rangle}{2 \langle O_b^2 \rangle^2} \right). \quad (\text{S12})$$

In Fig. 5d of the main text we showed how analysing  $U(J)$  for a range of system sizes allows an accurate determination of the location of the bicritical point for a fixed value of  $\Delta$ , as well as the value  $U_c$  there. In Fig. 5e we used the scaling collapse of  $U$  as another means of extracting  $\nu$ , and thereby demonstrating that the critical exponents take non-universal values. In Fig. S7b we show another example of the scaling collapse of  $U$ , prepared for a weak



$ i\rangle$	$ 1\rangle$	$ 2\rangle$	$ 3\rangle$	$ 4\rangle$
$ \sigma, \eta, \tau\rangle$	$ -1, +1, -1\rangle$	$ +1, +1, +1\rangle$	$ -1, -1, +1\rangle$	$ +1, -1, -1\rangle$

TABLE S2. Sets of Ising variables labelling the degenerate ground-state configurations of the effective classical model.

spin anisotropy of  $\Delta = 1.1$ , and in Fig. S7c we show the stronger spin anisotropy  $\Delta = 1.4$ . Taken together with Figs. 5d and 5e of the main text, these data form the basis of Fig. 5f, where we used  $U_c$  to show that the non-universal behaviour has a direct (linear) dependence on  $\Delta$ , reinforcing the expectation that the criticality of the model changes continuously between Ising and 4-state Potts universality. For an analytical understanding of this result we appealed to the fact that the Ashkin-Teller model (ATM) displays the same type of physics.

#### D. Ashkin-Teller model

Interpreting the non-universal behaviour of the bicritical point yields considerable insight into the emergent critical point. The ATM, defined in Eq. (3) of the main text, has non-universal critical exponents along a line of critical points as the model parameter ratio  $K/J$  is varied.<sup>42</sup> To examine the connection to the ATM, we map the anisotropic classical model of Eq. (S11) to an effective model valid around the transition where the x-Ising AFM and TC ground states are degenerate. Within each two-site unit cell one has two degenerate AFM ground states,  $|1\rangle = |\cos\theta T^z - \sin\theta T^x\rangle_A |\cos\theta T^z + \sin\theta T^x\rangle_B$  and  $|2\rangle = |\cos\theta T^z + \sin\theta T^x\rangle_A |\cos\theta T^z - \sin\theta T^x\rangle_B$ , and two degenerate TC ground states,  $|3\rangle = |s\rangle_A |T^z\rangle_B$  and  $|4\rangle = |T^z\rangle_A |s\rangle_B$ , where  $|s\rangle$  denotes a singlet state and  $T^x$  and  $T^z$  are components of the triplet operator.

These four ground-state configurations can be labelled by a set of three Ising variables,  $\sigma$ ,  $\eta$  and  $\tau$ , each of which takes the values  $\pm 1$ . The variable  $\sigma$  is associated with the sublattice symmetry  $A \leftrightarrow B$ , so that  $\sigma \propto (T_A^x - T_B^x)$  in the AF state and  $\sigma \propto (T_A^z - T_B^z)$  in the TC state. The variable  $\eta \propto \bar{T}_A^2 + \bar{T}_B^2 - 3$  is associated with the particle-hole symmetry about the triplet density  $n_t = 3/4$  per site of the square lattice, which arises when the relevant low-energy excitations are those associated with the AFM and TC phases. The third variable is  $\tau \equiv \sigma\eta$ , meaning that only any two out of the set  $\{\sigma, \eta, \tau\}$  are independent. The labelling of the states  $|i\rangle$  with the variables  $|\sigma, \eta, \tau\rangle$  is shown in Table S2.

These definitions allow us to construct the effective model. The sublattice symmetry requires this model to be invariant under  $\sigma \rightarrow -\sigma$  and the particle-hole symmetry requires it to be invariant under  $\eta \rightarrow -\eta$ . A minimal model with these symmetries is

$$H_{\text{eff}} = -J_\sigma \sum_{i,j} \sigma_i \sigma_j - J_\eta \sum_{i,j} \eta_i \eta_j - J_\tau \sum_{i,j} \tau_i \tau_j. \quad (\text{S13})$$

However, the original model is also invariant under the spin inversion  $T^x \rightarrow -T^x$ , which exchanges  $|1\rangle$  and  $|2\rangle$

while leaving  $|3\rangle$  and  $|4\rangle$  unchanged. In terms of  $\sigma$ ,  $\eta$  and  $\tau$ , this corresponds to  $\sigma \rightarrow -\tau$  and  $\tau \rightarrow -\sigma$ , and enforcing this symmetry in Eq. (S13) leads to  $J_\sigma = J_\tau = J$ . One may also make use of the identity  $\eta = \sigma(\sigma\eta) = \sigma\tau$ , so that Eq. (S13) can be rewritten with  $K = J_\eta$  as

$$H_{\text{eff}} = -J \sum_{i,j} (\sigma_i \sigma_j + \tau_i \tau_j) - K \sum_{i,j} (\sigma_i \tau_i \sigma_j \tau_j), \quad (\text{S14})$$

which is Eq. (3) of the main text.

Equation (S14) is precisely the ATM.<sup>42</sup> At  $K = 0$ , the ATM corresponds to two independent Ising models, and for  $0 < K \leq J$  it has a single finite-temperature transition, where in the low-temperature ordered phase  $\langle \sigma \rangle$ ,  $\langle \tau \rangle$  and  $\langle \sigma\tau \rangle$  are all non-zero. Most important from the perspective of the spin-anisotropic model is that when  $0 < K/J < 1$  this transition has non-universal properties, exhibiting critical exponents that vary continuously between Ising and 4-state Potts universality, the latter reached at  $K = J$ .

Returning now to our calculations, in Fig. 5f of the main text we compared the critical value,  $U_c$ , of the Binder cumulant at the bicritical points obtained for several different values of  $\Delta$  in the spin-anisotropic model [Eq. (S11)] with the  $U_c$  values at the critical points of ATMs with different  $K/J$ . When  $\Delta$  and  $K/J$  are scaled appropriately (the lower and upper axes of Fig. 5f), the  $U_c$  values of the two models coincide. Thus we confirm our conclusion that the non-universal behaviour of the bicritical point in the spin-anisotropic classical model can be described by the physics of the ATM. Finally, when the model is tuned to the isotropic limit ( $\Delta \rightarrow 1$ ), the extrapolated  $U_c$  we compute approaches the value  $U_c \simeq 0.792$  of the ATM at its isotropic point ( $K = J$ ),<sup>46,59</sup> where the universality class is 4-state Potts. Thus the ATM also describes the emergent criticality we observe in the classical models, and by extension in the quantum FFB model.

#### E. Conformal Field Theory

This extraction of the equivalent classical and effective critical models also sheds light on our result that the BKT transition of the DTAF phase has no effect on the universality classes of the critical lines of the FFB in a field. Critical theories in two-dimensional models are described by CFTs, from which it is found<sup>50</sup> that continuously varying critical exponents are possible when the conformal (central) charge of the CFT is  $c \geq 1$ , whereas transitions described by CFTs with  $c < 1$  are restricted to discrete critical exponents. In a conventional scenario where two symmetries, described separately by

CFTs with central charges  $c_1$  and  $c_2$ , are combined at a critical point, one might expect the relevant CFT to have  $c = c_1 + c_2$ , as in the well known FFX Y [U(1)⊗Z<sub>2</sub>] model.<sup>60</sup> However, the FFB model in a field turns out to be unconventional.

The Ising critical point of the spin-isotropic model at  $h = 0$  is described by a CFT with central charge  $c = 1/2$ . The BKT transition has XY universality, and hence is described by a  $c = 1$  CFT (free bosons). To understand our result in the low-field regime ( $h < h_{\text{tr}}$ ), it is instructive to consider the model with a finite spin anisotropy, such that the BKT transition is replaced by an Ising transition to true LRO: in this model, both at  $h = 0$  and at small finite  $h$ , the universality at the critical point becomes tricritical Ising, with  $c = 7/10$ . In the triplon basis, the Ising transition is driven by the triplet density,  $T^2$ , while in the presence of a spin anisotropy  $T_x$  is also a relevant operator, coupling to  $T^2$  by a term of the form  $-T_x^2 T^2$ . This coupling drives the tricritical Ising behaviour by changing the sign of the quartic term ( $T_x^4$ ), and one may view the transition as being driven by the triplon amplitude mode ( $|T_x|$ ). By contrast, the BKT transition is driven by the phase mode, which couples only marginally to  $T^2$ , this being invariant under a U(1) phase change. Thus one observes in the classical model how a BKT transition cannot have the same effect on the universality as a spin anisotropy, and instead leaves the critical properties in the same discrete (Ising) universality class as at  $h = 0$ .

At fields high enough that the phase transition is DTAF-TC, the sublattice symmetry becomes an additional relevant global symmetry. As shown above, this is represented by a second independent Ising variable, whence the appropriate effective theory is the ATM. The ATM with  $K \leq J$  is described by a  $c = 1$  CFT, meaning that continuously variable critical exponents are allowed, as we found in Fig. 5f of the main text both for the ATM

and for the classical model with spin anisotropy. However, the fact that the BKT transition has  $c = 1$  makes it only a marginally relevant perturbation of a  $c = 1$  theory, and thus its presence should have no effect on the approach of these exponents to their 4-state Potts values as  $K \rightarrow J$  in the ATM and as  $\Delta \rightarrow 1$  in the classical model. We conclude that the effect of the qLRO BKT phase on the critical properties of the FFB in an applied field is at most marginal, explaining why it has no effect on the universality classes we find.

## F. Summary

To summarize this analysis, we have employed the spin inversion, sublattice (or translational) and particle-hole (or singlet-triplet) symmetries to construct an effective ATM that describes the classical analogue of the FFB in the presence of an Ising spin anisotropy. For generic couplings, the ATM of Eq. (S14) does indeed have  $Z_2 \times Z_2 \times Z_2$  symmetry. However, when  $K/J = 1$  a higher  $S_4$  symmetry emerges, which allows a full permutation among the four degenerate ground-state configurations. It is easy to see that the spin-anisotropic model of Eq. (S11) has only the sublattice and spin-inversion symmetries ( $Z_2 \times Z_2$ ) of the generic ATM. In the isotropic limit, the spin-inversion symmetry is enhanced to a continuous O(2) (or U(1)) spin-rotational symmetry, but we stress that an  $S_4$  symmetry does not exist either in this classical Hamiltonian [Eq. (S10)] or in the original FFB model [Eq. (1) of the main text]. It is an emergent symmetry appearing only at the critical point of the DTAF-TC transition, and this is why we adopt the terminology of an emergent critical point.